Geological Survey of Japan Cruise Report No. 22, p. 145-217, 1992

X. REGIONAL AND LOCAL VARIATIONS OF MANGANESE NODULE DEPOSITS IN THE SOUTHERN PART OF THE CENTRAL PACIFIC BASIN (GH82-4 AREA)

Akira Usui

Introduction

Variations of manganese nodule deposits in abundance, coverage, morphology, chemistry, and mineralogy have been reported on various scales; from hundred meters (Andrews and Friedrich, 1979; Halbach and Özkara, 1979) to thousand kilometers (Mckelvey *et al.*, 1983). During the GH82-4 cruise conducted by Geological Survey of Japan (GSJ), regional and local variations of nodule deposits were investigated in the southern part of the Central Pacific Basin and in a small detailed survey area. Although this area may not be considered as a possible prime mining area, a small-scale geological mapping of manganese nodule field is significant in understanding genesis of manganese nodules and mineral exploration. GH82-4 area is the third model site of our program (1979 to 1983) on the Wake-Tahiti Transect (Fig. X-1). The objective of this survey is to characterize the regional and local variation patterns of manganese nodule facies and to relate them to sedimentary conditions.

Methods

Reconnaissances seismic survey and sampling were done during the first leg of the cruise using free-fall grabs at 49 stations. Station intervals are about 10 nautical miles (approximately 18 km). During the second leg, nodule and sediment sampling were carried out in the detailed survey area located in the eastern part of the regional survey area by using free-fall grab, piston corers, box corers and dredges. The shortest station interval in the detailed survey area is around one kilometer which is nearly equal to the maximum ship positioning error at that time. Methods of sampling, sea-bed photography, and on-board description employed are same as those during the cruises GH80-5 (Usui and Nakao, 1984) and GH81-4 (Usui, 1986; Usui *et al.*, 1987).

Survey areas

The GH82-4 area (0°20′N-2°40′S, 165°40′W-169°00′W) is located at the equatorial zone of the Central Pacific Basin. This area is terminated to the north by the Nova-Canton Trough and is located about three hundred kilometers to the north of the Manihiki Plateau. The area may be divided into following three topographic provinces: steep ridges and depressions of the Nova-Canton Trough, western flat basins, and eastern rugged abyssal hill area. The topographic lineation is nearly parallel to the

Keywords: manganese nodule, abundance, sea-bed photography, hydrogenetic, diagenetic, regional variation, small-scale variation, Central Pacific Basin, Hakurei-Maru, Nova-Canton Trough

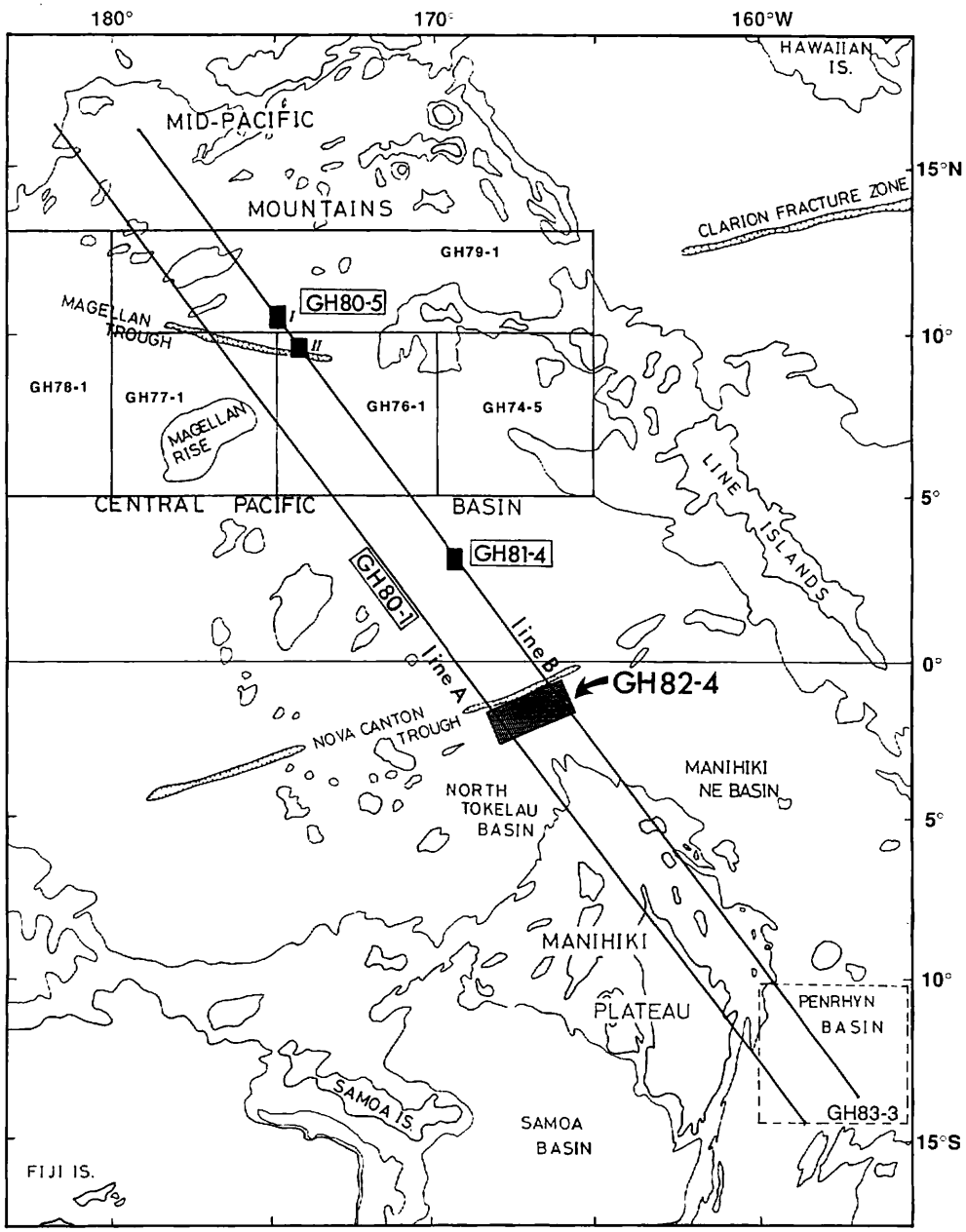

Fig. X-1 Location map of survey areas of GH82-4 cruise and earlier study areas by GSJ. Base map modified from Chase *et al.* (1977) published by Scripps Institution of Oceanography. Contours denote 2000 and 2600 fathoms.

axis of the trough in the western part but normal to the axis in the eastern part (Tanahashi, chapter IV of this volume). Most of the GH82-4 area is covered with surface siliceous ooze or clay, though older consolidated sediments or basement rocks are in places exposed in the vicinity of the trough. Topographic highs of which water depth is less than 5000 meters are covered with calcareous surface sediment in the regional and detailed survey areas (Nishimura and Ikehara, chapter VI of this volume).

This area includes earlier sampling Stations 1605, 1606, 1630, and 1631 along the Wake-Tahiti Transect of the GH80-1 cruise (Usui, 1983), where a local variation of nodule facies has been suggested. The detailed survey area (0°45′S-1°05′S, 166°05′W-166°30′W) was selected in the eastern part of the GH82-4 area. This area includes two seamounts at the northwestern corner and in the southern part. Small basins and abyssal hills are present in the middle and eastern parts. The maximum elevation from the basins is around 1700 m. Short-scale sampling were made along twelve lines combining two known sample stations at 5-mile intervals (Fig. X-2).

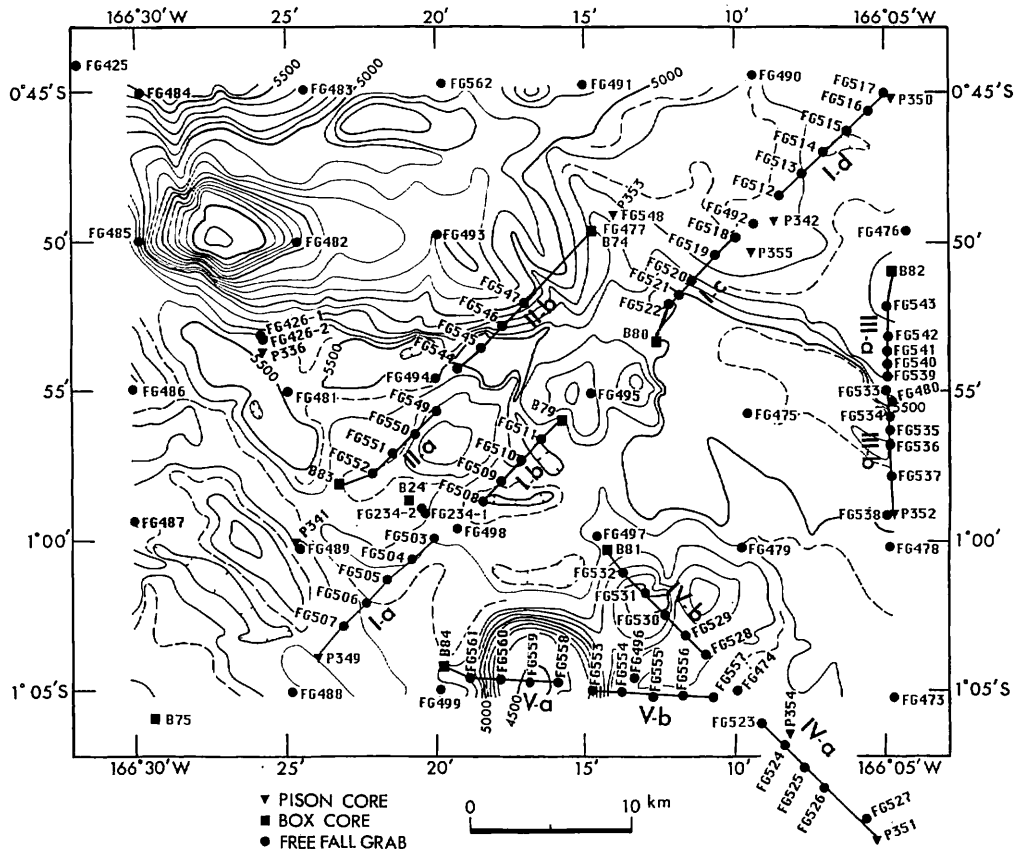

Fig. X-2 Topography and sample location of the detailed survey area. Each combined line shows a set of small-scale sampling by free-fall grabs.

Acoustic and bathymetrical survey was carried out at 6 to 30-mile intervals during the regional survey and at 2.5 to 5-mile intervals in the detailed survey area. Seismic profile records reveal that the structure is considerably variable within the GH82-4 area. The uppermost transparent layers are widely distributed in this area. They may be correlated to the Unit I consisting of acoustic transparent layers defined in the northern Central Pacific Basin and can be correlated to siliceous oozes and clays from the Oligocene to the Recent (Tamaki *et al.*, 1977). Acoustic basement is locally exposed at steep flanks of abyssal hills and near the Trough, some of which may be identifiable as outcrop of basaltic basement (Tanahashi, chapter IV of this volume).

Nodule occurrence and morphology

Among 177 sampling operations, 119 samplers (98 free-fall grabs, 11 box cores, 8 piston cores, and 2 dredges) recovered manganese nodules from the sea bed. Occurrence of nodules on sediment surface were viewed by one-shot cameras fixed to free-fall grabs or box corers, and observed at recovered box cores on deck. Nodule abundance, sea-floor coverage ratio, external morphology, sea-bed occurrence, and other on-board data are listed in Appendix X-1 and X-2.

The criteria for on-board nodule description established during previous GSJ cruises in the northern Central Pacific Basin (Moritani *et al.*, 1977) was adopted again and proved available in describing GH82-4 nodules. Nodules were classified according to surface structure into type s (smooth surface nodules), type r (rough surface nodules), and type s.r (nodules of intermediate surface feature). Intermediate feature is due to recent change in depositional environment as revealed by microscopical study of polished cross sections (Usui, chapter XII of this volume). As very few nodules from this area are of different surface structure between top side (in contact with sea water) and bottom side (with sediments) sides on the sea floor, most nodules were classified into one of three morphological types.

Sea-bed photographs and on-site observation of box core surface show a markedly different occurrences with nodule type. Typical rough surface nodules (type r) are commonly buried within top siliceous sediments at several centimeters depths. For instance, at Stations FG492 and FG516, many nodules of Sr and Dr (abundance: 5.1, 7.5 kg/m^2, respectively) were collected in spite of no visible nodule on sea-bed photographs (coverage=0 %). On the other hand, type-s nodules on the sea floor are usually exposed to sea water, and are always visible on sea-bed photographs (e.g., FG459, FG488). Figure X-3 showing the relationship between nodule abundance and coverage well demonstrates buried feature of type-r nodules.

Frequency distribution of abundance (Fig. X-4) and size (Fig. X-5) demonstrate that each type has characteristic ranges. The size of type r is relatively small ranging from less than 0.5 cm to 2.5 cm, and the abundance quite variable. The shape is mostly spherical or discoidal, and mononucleated nodules are dominant.The size of type s is relatively large; the maximum diameter greater than 2 cm. Their abundance is relatively great. The shape is various, and polynucleated feature is dominant. Intermediate type generally has intermediate features between type s and type r in terms of sea-bed occurrence, size, and abundance.

These tendency of sea-bed occurrence and physical characteristics of manganese

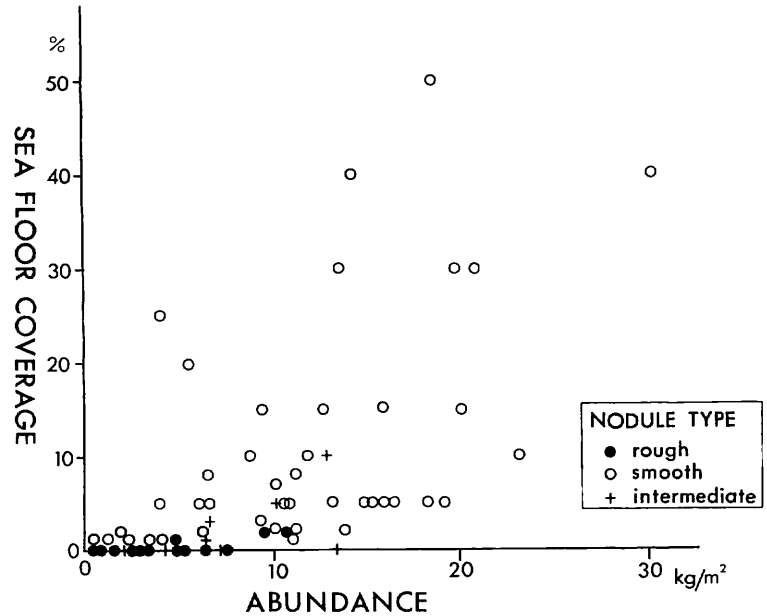

Fig. X-3 Relationships between nodule abundance and sea-floor coverage ratio, showing marked differences with nodule type.

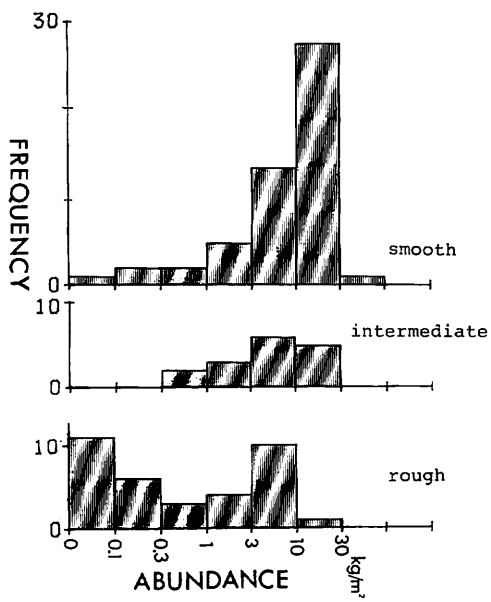

Fig. X-4 Frequency distribution of nodule abundance. Frequency is shown in numbers of stations of nodule occurrence.

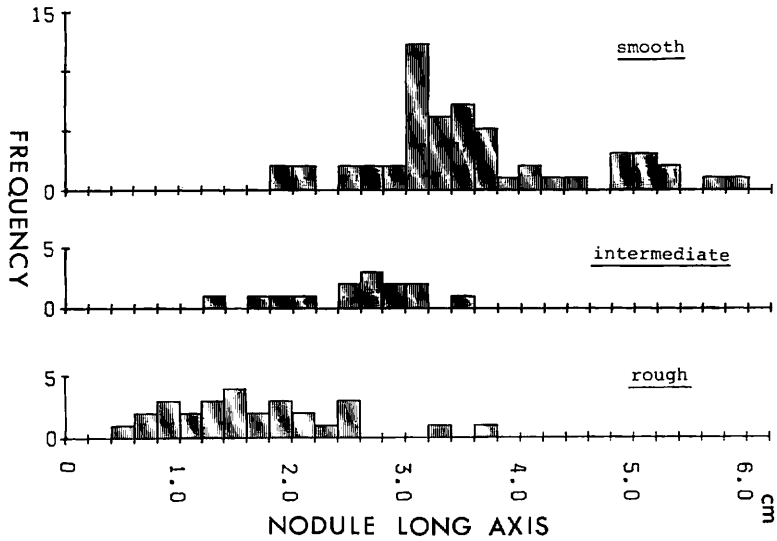

Fig. X-5 Frequency distribution of nodule diameter. Nodule long axis is represented by median values of the longest diameters in each station. Frequency is shown in numbers of station of nodule occurrence.

of the GH82-4 area is generally common to those found in the northern Central Pacific Basin during our previous cruises (Moritani *et al.*, 1977; Usui, 1983; Usui *et al.*, 1987). Table X-1 summarizes characteristics of the two types taking previous results into account.

Regional and local variations of manganese nodule facies

It was found during the GH80-1 research cruise on the Wake-Tahiti Transect (4000 km long) that nodule morphology varies from type s to type r in accordance with four geologic provinces in the Central Pacific Basin. This regional variation of nodule type is determined by nodule mineralogy resulting in different nodule growth structure and compositions (Usui and Mochizuki, 1982). In the GH82-4 area a great regional variation of nodule type was again found on a scale of hundred kilometers during regional survey and on a scale of several kilometers during detailed survey.

Regional variation in the GH82-4 survey area

A regional pattern of variation of manganese nodule facies (Fig. X-6) shows that nodules are most abundant in the eastern abyssal hill area of rolled topography. The abundance often exceeds 10 kg/m^2, while their morphology (type s, type r, intermediate) is variable. In contrast, only type-r nodules are distributed in the western flat basin area with very low abundance. The southern ridge of the Nova Canton Trough yields local great abundance of type s and manganese crusts associated with thin calcareous clay sediment and basement hard rocks.

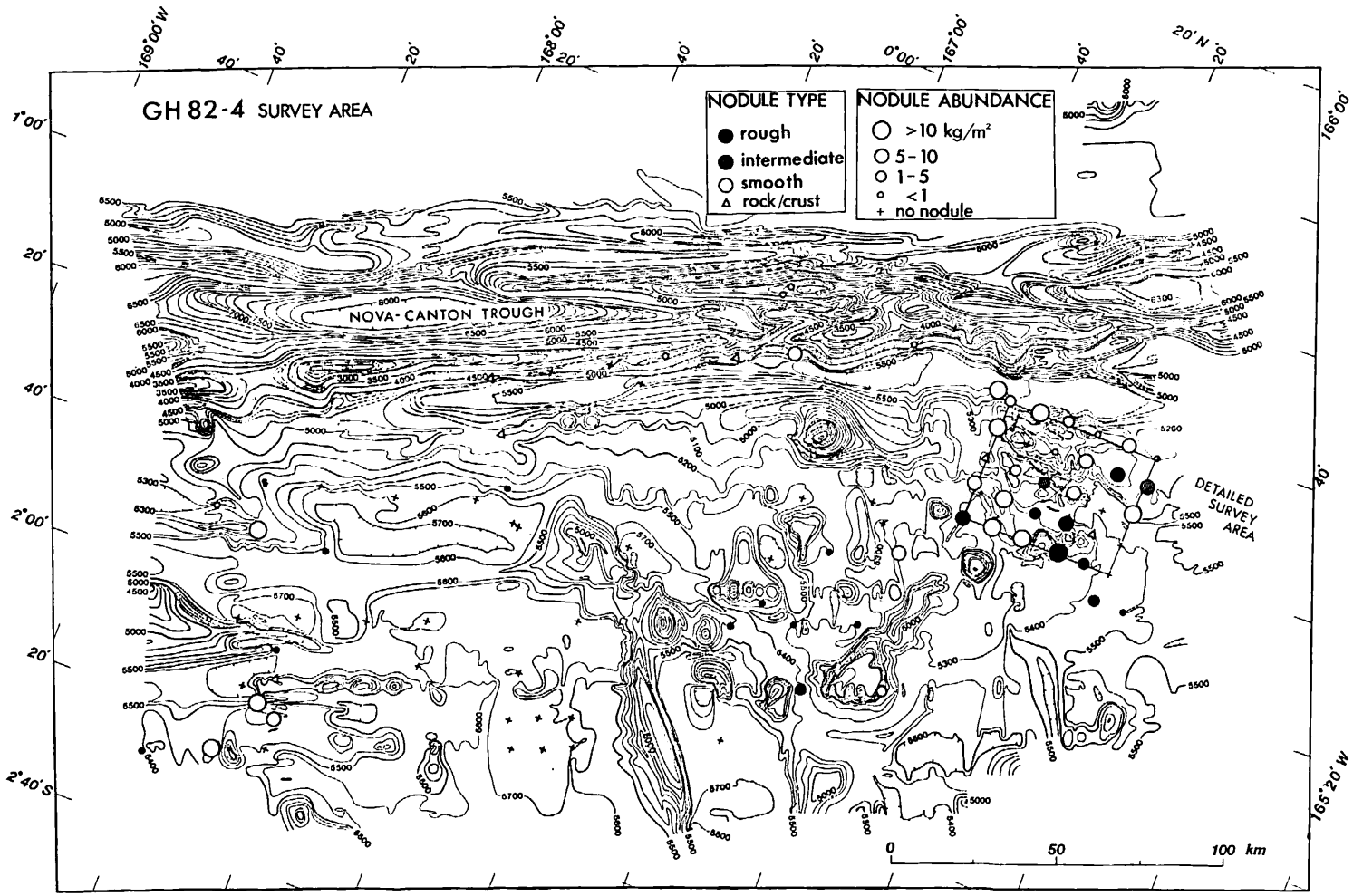

Fig. X-6 Distribution of manganese nodules in the GH82-4 area. Data of small-scale sampling in the detailed survey area are not included.

This regional distribution patterns appear to be generally related to three general topographic provinces. Abundant nodule deposits in the east are related to slow sedimentation in basin areas, and a local high abundance is similarly related to no sedimentation or erosion in topographic highs. Very flat abyssal plain in the west influenced by calcareous turbidite deposits derived ambient island chain may have prevented nodules to grow.

Local variation in the detailed survey area

The detailed survey area seems the most abundant nodule field in the GH82-4 area. The grid survey and sampling at 5-mile intervals and short scale sampling at 1-mile interval suggest abundant but variable nodule distribution on a kilometer scale within this small area (Fig. X-7). No or scarce nodules are distributed on the top and flank of two seamounts which elevate above CCD. Nodules are scarce in the the southeastern basins where uppermost transparent layer is thick. Abundant nodule deposits (ranging from 5 to 30 kg/m^2) are related to rolled topography irrespective of variable morphological type. It appears in general that the distribution of s-type nodules is related to slightly elevated topography and that of r-type nodules to small basins. However, this relationship is not always applied exceptionally around the northeastern height,where type r and intermediate nodules are abundant but type s is distributed in the southern scarped slopes. The different pattern of local variation is very similar to that found around the small abyssal hills in the GH81-4 survey area (centered at 3°00′N, 169°30′W, Usui *et al.*, 1987). The pattern of variation in the detailed survey area suggests that variation in nodule abundance and morphology are not simply controlled by water depth or topography in this area. The variation may be more closely related to sedimentary history during the Neogene and Quaternary Periods, as pointed out during our previous detailed surveys in the Central Pacific Basin (Mizuno *et al.*, 1980; Usui *et al.*, 1987). The relationship between nodule facies and acoustic stratigraphy is in further details discussed in chapter XI (Usui and Tanahashi, this volume).

Buried nodules

Nine sediment cores contained buried nodules within siliceous clay and ooze (Appendix X-3). They are considered to have been rested on then sea bed and later overlain by younger sediments. Four box cores (B75, B79, B80, B84) and five piston cores (P342, P349, P350, P353, P355) contain manganese nodules at various depths below sea floor.

The nodules from four box cores are similar in diameter, shape, and depth below the sea floor. The distances between locations are within several kilometers. It would be possible that these nodules are correlated to each other in time (Nishimura and Ikehara, chapter XI of this volume), though stratigraphic investigations of associated sediments are needed in further details.

Nodules from four piston cores are less abundant and much smaller in size. The depths of occurrence are variable. It appears that these nodules occur at upper horizons than the boundary between the upper siliceous clay and the lower siliceous ooze. Nishimura and Ikehara (chapter VI, this volume) stated that the boundary

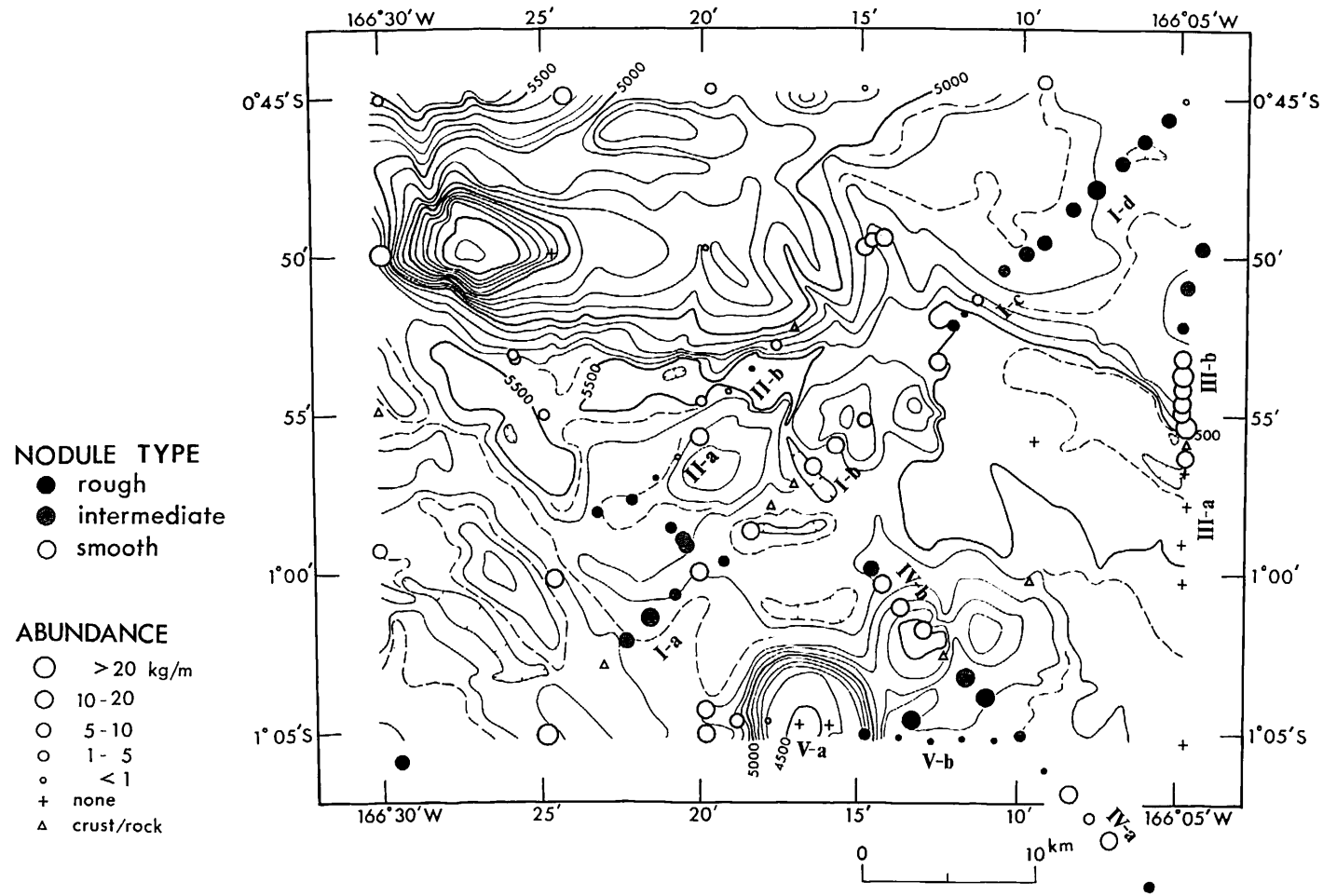

Fig. X-7 Distribution of manganese nodules in the detailed survey area.

represents the hiatus caused by the strengthened current originated from the Antarctic Bottom Waters in the early-middle Miocene to the early Pleistocene.

Summary

Reconnaissance and small-scale nodule sampling and observation with sea-bed photographs have shown a general pattern of variation of nodule facies in the south of the Nova-Canton Trough, equatorial Central Pacific Basin. Nodules are most abundant in the eastern rolled abyssal hill area but scarce in the western flat basin area.

The criteria of morphological classification of nodules previously established in the northern Central Pacific Basin proved applicable to nodules of this area. The types s and r have characteristic morphology and sea-bed occurrences, in spite of their great areal distributions.

Nodule abundance, morphology, and occurrence are variable on the scale of several kilometers in the detailed survey area. Abundant nodule deposits are apparently related to rolled topography of the sea floor with thin transparent layers, and flat basins where calcareous turbidite is dominant yield scarce nodules. On the other hand, nodule morphology (surface structure) is much more variable within rolled topography areas, although nodule abundance is fairly constant. The mode of variation of nodule morphology seems to be very weakly related to water depth, topography, or sediment type. Sedimentary history of the nodule field may be most important factor controlling nodule morphological type.

References

Andrews, J. E. and Friedrich, H. W. (1979) Distribution patterns of manganese nodule deposits in the Northeast Equatorial Pacific. *Marine Mining*, vol. 2, no. 1/2, p. 1-43.

Halbach, P. and Özkara, M. (1979) Morphological and geochemical classification of deep-sea ferromanganese nodules and its genetic interpretation. In: C. Lalou (ed.), La Genèse des Nodules de Manganèse. *C. N. R. S. Rept.*, no. 289, p. 77-88.

McKelvey, V. E., Nancy, A. W. and Bowen, R. W. (1983) Analysis of the World Distribution of Metal-Rich Subsea Manganese nodules. *Geological Survey Circular 886*, U.S.G.S., 55 p.

Mizuno, A., Miyazaki, T., Nishimura, A., Tamaki, K. and Tanahashi, M. (1980) Central Pacific manganese nodules, and their relation to sedimentary history. *Proc. Offshore Technology Conference in Houston, May 5-8, 1980*, (OTC3830), p. 331-340.

Moritani, T., Maruyama, S., Nohara, M., Matsumoto, K., Ogitsu, T. and Moriwaki, H. (1977) Description, classification, and distribution of manganese nodules. In: Moritani, T. (ed.), *Geol. Survey Japan Cruise Rept.*, no. 8, p. 136-158.

Tamaki, K., Joshima, M. and Larson, R. L. (1979) Remanent Early Cretaceous spreading center in the Central Pacific Basin. *J. Geophys. Res.*, vol. 84, p. 4501-4510.

Usui, A. (1983) Regional variation of manganese nodule facies on the Wake-Tahiti

Transect: morphological, chemical and mineralogical study. *Mar. Geol.*, vol. 54, p. 27–51.

——— (1986) Local variability of manganese nodule deposits in the GH81–4 area. In: Nakao, S. (Ed.), *Geol. Survey Japan Cruise Rept.*, no. 21, p. 98–159.

———, Nishimura, A., Tanahashi, M. and Terashima, S. (1987) Local variability of manganese nodule facies on small abyssal hills of the Central Pacific Basin. *Mar. Geol.*, vol. 74, p. 237–275.

——— and Mochizuki, T. (1982) Regional variation of manganese nodule chemistry from Wake to Tahiti, GH80–1 cruise. In: Mizuno, A. and Nakao, S. (eds.), *Geol. Survey Japan Cruise Rept.*, no. 18. p. 338–354.

——— and Nakao, S. (1984) Local variability of manganese nodule deposits in the GH80–5 area. In: Nakao, S and Moritani, T. (eds.), *Geol. Survey Japan Cruise Rept.*, no. 19, p. 106–164.

Appendix X-1 Sample list and results of shipboard observations of manganese nodules.

STA	SAM	COV		SED	NOD-TYPE	ABD	10	8	6	4	2	1	0	WT	INTERNAL	NUCLEI	POLY	REM [POSITION]
3246	FG424	0	H	-		0.0								0				
3247	FG425	-	-	sC	SPs, ISPs, Ts	16.0				29	53			1851	dense layers surrounding broken nodule	zeolitic claystone	90	
3248	FG426-1	1	L	sC	IDs, Fs, Is	4.0			1	4	15	5		467	dense layers surrounding broken nodule	zeolitic claystone	0	basalt, shark tooth
	FG426-2	1	L	sC	IDs, Is	3.4				1	58	11		391	dense layers surrounding broken nodule	zeolitic claystone	0	basalt, brown rocks
	P336	-	-	sC	IDs	-					1			11			0	
3249	FG427	0	L	sC	DPs	tr						1		1			100	zeolitic claystone
	B70	-	-	-		-								0				
3251	FG428	-	-	sC	IDs, IDPs, Ts, Fs	5.7				2	76	74	10	661	dense layers surrounding broken nodule	zeolitic claystone	50	
3252	FG429	R/C	-	-		0.0								0				
3253	FG430	0	M	cO	Vs	tr							1	1			0	
	B71	0	-	cO	Vs	tr							1	1			0	benthic foram [buried]
3254	FG431	1	M	cO	IDs, DPs	0.4				1	2	6		42	dense layers	brown claystone	20	
3255	FG432	0	M	cO		0.0								0				
3256	FG433	-	-	-		0.0								0				
3257	FG434	0	M	cO		0.0								0				
3258	FG435	R/C	H	-	IDs, Fs	1.5		1			3	4		174	dense layers surrounding broken nodule	zeolitic claystone	0	
3259	FG436	R/C	H	-		0.0								0				
3260	FG437	0	L	sC	Sr?	tr							1	1			0	pumice
3261	FG438	0	L	sC		0.0								0				
3262	FG439	-	-	sC		0.0								0				
	P337	-	-	sC	IDs.r	-					2			30		zeolitic rock?	0	
3263	FG440	0	L	sC		0.0								0				pumice, shark tooth
3264	FG441	0	L	sC		0.0								0				
3265	FG442	0	L	sC	Sr?	tr							1	1			0	
	P338	-	-	sC		-								0				
3266	FG443	0	-	cO		0.0								0				benthic foram
3267	FG444	15	-	cO	IDs, IDPs, Ts, Fs	15.8		1	3	39	28			1826	dense layers surrounding broken nodule	angular brownish rock	30	
3268	FG445	0	L	sC	Ds, IDPs, Fs	0.4					4			43	dense layers surrounding broken nodule		30	
3269	FG446	0	L	sC		0.0								0				
3270	FG447	-	-	-		0.0								0				
3271	FG448	0	-	sC		0.0								0				
	FG72	0		sC		0.0								0				
3272	FG449	0	0	sC		0.0								0				pumice
3273	FG450	0	0	sC		0.0								0				sponge
3274	FG451	0	L	sC	(Ir)	tr							1	1			0	zeolitic claystone

Appendix X-1 (continued)

STA	SAM	COV		SED	NOD-TYPE	ABD	10	8	6	4	2	1	0	WT	INTERNAL	NUCLEI	POLY	REM [POSITION]
3275	FG452	1	M	sC	IDs, Ts, Is	2.3			4	5	1	2		266	dense layers surrounding broken nodule and rocks	zeolitic claystone	10	
3276	FG453	0	L	sC	Ir, Sr	0.1				1		2		16	thin laminated layers	pumice	0	shark tooth
3277	FG454	-	-	sC	Sr	3.5			1	1	10	40	27	399	concentric and laminated	shark tooth	0	
	P339	-	-	sC		-								0				
3278	FG455	-	-	sC	Sr	0.1						3	1	7			0	
3279	FG456	-	-	sC	Sr, Ir	tr						3	3	3			0	
3280	FG457	0	L	sC	Vr, Sr	tr						5	6	4			0	
3281	FG458	0	L	sC		0.0								0				pumice
3282	FG459	50	L	sC	IDs, IDPs	18.6			2	27	93			2145	dense layers surrounding broken nodule and rocks	claystone	20	
3283	FG460	0	L	sC	Sr, Vr	tr					1		3	4	concentric and laminated	none or small	0	
	B73	0	-	sC	Vr	tr						3		3			0	pumice [buried]
3284	FG461	3	L	sC	Is.r, Ds.r	9.3			3	16	47	1	1	1072	dense layers surrounding concentric nodule	none or small	30	
3285	FG462	R/C	H	-		0.0								0				
3286	FG463	0	L	sC		0.0								0				
3287	FG464	30	M	sC	IDPs, DPs	19.8	1	3	3	18	92	4		2290	dense layers surrounding broken nodules	brown rocks	80	
3288	FG465	0	L	sC		0.0								0				Mn-coated pumice
	P340	-	-	sC		-								0				
3289	FG466	0	L	sC		0.0								0				
3290	FG467	0	-	sC		0.0								0				pumice
3291	FG468	0	L	sC		0.0								0				
3292	FG469	0	-	sC		0.0								0				
3293	FG470	0	L	sC		0.0								0				
3294	FG471	0	L	sC		0.0								0				
3295	FG472	0	L	sC	Sr	0.4					4	2	7	49	concentric and laminated	none or small	0	shark tooth
3296	FG473	0	L	sC		0.0								0				
3297	FG474	0	L	sC	Sr	2.9				1	18	9	1	339	concentric and laminated	none or small	0	
3298	FG475	0	L	sC		0.0								0				
3299	FG476	0	L	sC	Ss.r	7.1					61	71	2	821	concentric and laminated; dense outer layers	none or small	10	
3300	FG477	10	H	sC	SPs	8.7				6	59			1004	dense layers surrounding concentric nodule	none or small	80	
	B74	8	M	sC	SPs	11.2								1707	dense layers surrounding concentric nodule	none or small	90	[exposed]
3301	FG478	0	L	sC	(Vr)	tr						1		2			0	
3302	FG479	R/C	-	-		0.0								0				
3303	FG480	40	M	-	ISs	30.3	1	0	12	11	4			3505	dense and massive	zeolitic rock	0	
3304	FG481	0	M	sC	IDs	1.2				2				142	dense layers surrounding broken nodule	brownish rock	0	
3305	FG482	0	H	cO		0.0								0				
3306	FG483	1	H	pC	ISs, IDPs, Fs	11.0			1	11	33	64	5	1273	dense layers surrounding broken nodule	brownish rock	10	
3307	FG484	1	L	-	IDPs,IDs, ISs	1.3					9			146	dense layers slightly laminated	brownish rock	80	
3308	FG485	15	M	scO	IDs, Fs	20.1			1	17	47	30		1718	dense layers surrounding broken nodule	none or small	20	

Appendix X-1 (continued)

STA	SAM	COV		SED	NOD-TYPE	ABD	10	8	6	4	2	1	0	WT	INTERNAL	NUCLEI	POLY	REM [POSITION]
3309	FG486	R/C	-	sC		0.0								0				
3310	FG487	5	L	scO	IDs, IDPs	6.0			1	11	20			766	dense layers surrounding broken nodule and rocks	zeolitic rock	30	
3311	FG488	30	H	scO	ISs, IDs	20.8	1	0	1	20	5			2408	dense layers surrounding broken nodule and rocks	zeolitic rock	20	
3312	FG489	5	L	-	IDs, Ds, IDPs	14.7		5	7	13	10			1697	dense layers surrounding broken nodule and rocks	brownish rock	30	
	P341	-	-	sC	Ss, SPs	-					3			34			30	
3313	FG490	15	H	scO	SPs, DPs	9.5				20	38			1103	dense layers surrounding concentric nodule	brownish rock	90	
3314	FG491	0	-	cO	Ss	0.2					3			19	concentric and laminated	none or small	30	
3315	FG492	0	-	scO	Sr	5.1					51	48	3	595	concentric and laminated	none or small	10	
	P342	-	-	csC		-								0				[3 buried nods; -465, -637,-768cm
3316	FG493	0	M	-	ISs	0.2				2	1			28	dense layers surrounding concentric nodule	brownish rock	0	
3317	FG494	0	L	csC	Ds.r, DPs.r	4.3			2	3	20	5		493	concentric and laminated	none or small	30	
3318	FG495	2	M	cO	IDPs, Ts	8.2			3	12	18	5		952	dense layers surrounding dense nodule	zeolitic rock	60	
3319	D513	-	-	-	Sr	-								60 kg	concentric and laminated	none or small		shark tooth, whale bone
3320	FG496	0	L	-	IDs.r, IDPr	13.2		2	8	6	0	1		1525	dense or laminated; asymmetric	zeolitic claystone	0	
3321	FG497	2	L	cO	Sr, SPr	9.5					80	112	30	1090	concentric and laminated	none or small	10	
3322	FG498	1	-	sC	Sr	4.4					30	18		510	concentric and laminated	none or small	0	pumice
3323	FG499	5	-	-	ISPs, IDs	14.2			2	27	70			1636	dense layers surrounding broken nodule and rocks	zeolitic claystone	80	
3324	B75	0	-	sC	IDr, Dr, IDPr, Sr	6.3			1	18	27	9	3	951	laminated layers surrounding broken nodule	none or small	10	[mostly buried]
	B75X	-	-	-	IDr, IDPr, Dr	-				4	1			211	laminated layers surrounding broken nodule	zeolitic rock	0	[-15 cm depth]
3325	P343	-	-	sC		-								0				
3326	P344	-	-	sC		-								0				
3327	B76	0	L	sC		0.0								0				
3328	P345	-	-	sC		-								0				
3329	FG500	0	-	sC		0.0								0				
	P346	-	-	csC		-								0				
3330	B77	0	-	sC		0.0								0				pumice
3331	FG501	1	-	-	IDs, IDPs	5.2				5	15			600	dense layers surrounding broken nodule	none or small	10	
	P347	-	-	csC	Ss, DPs	-					2	1		20	dense layers surrounding concentric nodule	none or small	70	
3332	FG502	0	-	sC		0.0								0				
	P348	-	-	sC		-								0				
3333	B78	0	-	sC	Sr	0.1							20	8	concentric and laminated	none or small	0	shark tooth [buried]
3334	FG503	30	-	sC	IDs, IDPs	13.6			3	18	40	10		1573	dense layers surrounding broken nodule	brownish rock	30	
3335	FG504	0	L	sC	ISs.r, Sr	1.4			1	0	1	5	5	166	concentric and laminated	pumice	0	
3336	FG505	10	L	sC	Ss.r, SPs.r	12.8				3	133	40		1475	dense layers surrounding concentric nodule	none or small	60	
3337	FG506	3	M	sC	Ss.r, SPs.r	6.0					50	138	21	690	dense layers surrounding concentric nodule	none or small	20	
3338	FG507	-	-	sC		0.0								0				
	P349	-	-	sC	SPs, ISPs	-					5			55	dense layers surrounding concentric nodule	none or small	40	[1 buried nod; -153 cm]
3339	FG508	5	H	-	IDPs, IDs	18.2			4	16	7			2108	dense layers surrounding broken nodule	brownish rock	30	

Appendix X-1 (continued)

STA	SAM	COV	SED	NOD-TYPE	ABD	10	8	6	4	2	1	0	WT	INTERNAL	NUCLEI	POLY	REM [POSITION]
3340	FG509	N/C	-	-	-							1	1	laminated	brownish rock	0	
3341	FG510	N/C	H	-	IDs	>0.3				1			33	dense layers surrounding broken nodule	brownish rock	0	
3342	FG511	15	H	sC	IDs, IDPs	12.6			1	16	27	1	1455	dense layers surrounding broken nodule	zeolitic claystone	20	
3343	B79	5	-	sC	IDs, IDPs	16.4		2	7	17	38	3	2494	dense layers surrounding broken nodule	zeolitic claystone	60	[exposed]
	B79X	-	-	-	IDr+s	12.2	4	2	0	0	1		1414	dense layers surrounding rocks	zeolitic claystone	0	benthic foram [-12 cm depth]
3344	FG512	-	-	sC	Sr, SPr	7.9				1	64	75	1	909	concentric and laminated; outer dense layers	none or small	20	shark tooth
3345	FG513	-	-	sC	Ss.r	16.1				3	127	46		1860	concentric and laminated; outer dense layers	none or small	10	
3346	FG514	2	L	scC	Ss.r, SPs.r	9.6				1	97	19		1113	concentric and laminated; outer dense layers	none or small	30	
3347	FG515	0	L	scC	Sr	5.1					45	46	3	592	concentric and laminated	none or small	0	shark tooth
3348	FG516	0	L	scC	Sr	7.2					74	46	7	834	concentric and laminated	none or small	0	
3349	FG517	2	-	-	SPs.r, ISs.r	0.6					8	2		75	concentric and laminated; outer dense layers	none or small	40	
	P350	-	-	sC	Ss.r	-					2	1		24	concentric and laminated; outer dense layers	none or small	0	[1 buried nod; -172 cm]
3350	FG518	0	L	scO	SPs, Ss, ISPs	7.1				3	53	3		815	concentric and laminated; outer dense layers	none or small	30	
3351	FG519	0	L	scO	Ss.r	2.8					24	9		322	concentric and laminated; outer dense layers	none or small	0	
3352	FG520	25	H	sC	IDPs, IDs, ISPs	4.0			2	3	16			459	dense layers surrounding broken nodule	zeolitic rock	70	
3353	FG521	0	L	sC	Sr, Dr, Vr	0.5					5	5	2	57	concentric and laminated	none or small	5	
3354	FG522	0	-	sC	Sr, Dr	3.1				4	7			355	concentric and laminated	none or small	0	
3355	B80	10	-	sC	IDPs, ISPs, IDs	10.9			3	18	4			1661	dense layers surrounding broken nodule	brownish rock	20	[exposed]
	B80X	-	-	-	ISs, IDs	10.9			7	7				1653	dense layers surrounding broken nodule	zeolitic claystone	10	[-15 cm depth]
3356	FG523	0	L	-	(Sr)	tr							1	<1			0	
3357	FG524	5	-	sC	Ts, IDs, Ts+r	14.3		1	4	6	17	11		1657	dense layers surrounding rocks	zeolitic rock	0	
3358	FG525	5	H	sO	Ts, IDs	4.0			2	7	2			463	dense layers surrounding rocks	zeolitic rock	0	
3359	FG526	2	M	sC	IDs, Ts, Ts+r	10.0			8	15	10			1158	dense layers surrounding rocks	zeolitic rock	0	
3360	FG527	0	L	sC	Sr, Dr	4.9			1	1	23	43	37	563	concentric and laminated	none or small	0	
	P351	-	-	sC		-								0				
3361	FG528	2	L	sC	Sr, Dr	10.5				3	62	37	5	1213	concentric and laminated	none or small	0	
3362	FG529	5	-	sC	Ss.r, SPs.r	10.1				1	115	97	11	1166	concentric and laminated; outer dense layers	shark tooth	30	shark tooth
3363	FG530	R/C	-	-		0.0								0				
3364	FG531	2	L	sC	ISs	11.6				10	17	1		1344	dense layers surrounding broken nodule	zeolitic rock	10	
3365	FG532	5	-	sC	IDs, TS, IDPs	10.8			6	17	57	3		1247	dense layers surrounding broken nodule	zeolitic rock	30	
3366	B81	7	M	sC	SPs, Ss	10.1				18	98	9		1537	dense layers surrounding concentric nodule	none or small	70	shark tooth [exposed]
3367	FG533	40	H	sC	IDs, IDPs	14.4				18	71	45		1662	dense and laminated	zeolitic rock	40	
3368	FG534	R/C	-	-		0.0								0				
3369	FG535	5	H	sC	IDPs, IDs	14.9		2	5	13	17			1726	dense layers surrounding broken nodule	zeolitic rock	60	
3370	FG536	0	L	-		0.0								0				
3371	FG537	0	L	sC		0.0								0				
3372	FG538	0	L	sC		0.0												
	P352	-	-	sC		-												

Appendix X-1 (continued)

STA	SAM	COV	SED		NOD-TYPE	ABD	10	8	6	4	2	1	0	WT	INTERNAL	NUCLEI	POLY	REM [POSITION]
3373	FG539	5	M	sC	IDs, IDPs	10.5				20	38			1210	dense layers surrounding broken nodule	brownish rock	50	
3374	FG540	8	-	sC	IDs, IDPs	6.5			1	17	27			753	dense layers surrounding broken nodule	none or small	50	
3375	FG541	10	-	-	ISs, IDs	23.1		1	10	13	3			2672	dense layers surrounding broken nodule	brownish rock	10	
3376	FG542	5	L	sC	IDs, ISs, IDPs	18.3			3	29	32			2121	dense layers surrounding broken nodule	brownish rock	30	
3377	FG543	0	L	sC	Is.r, Fs.r	2.3	1	0	0	1	3	1	1	269	laminated layers surrounding broken nodule		0	
3378	B82	1	-	sC	Ss.r, SPs.r, Ds.r	6.3					97	39	2	955	concentric and laminated	none or small	50	[mostly exposed]
3379	FG544	5	M	sC	ISs, IDs, Fs	6.0			3	3	7			969	dense layers surrounding broken nodule	zeolitic rock	30	
3380	FG545	0	L	sC	Sr	0.1						3	2	7	concentric and laminated	none or small	0	
3381	FG546	2	-	-	IDs, Fs	1.9				3	17	4		222	dense layers surrounding broken nodule	none or small	10	
3382	FG547	R/C	-	-		0.0								0		none or small		
3383	FG548	5	M	cC	SPs, ISPs	13.2				20	77	1		1523	dense layers surrounding concentric nodule	none or small	100	
	P353	-	-	sC	IDs, IDPs, ISPs	-					3			33	concentric and laminated	none or small	70	[1 buried nod; -535 cm]
3384	FG549	2	L	sC	IDPs, ISPs, IDs	13.8				4	127	8		1600	dense layers surrounding concentric nodule	none or small	60	
3385	FG550	0	L	sC	Is	tr						1	1	2			50	
3386	FG551	0	L	sC	Sr	tr						4	3	4	concentric and laminated	none or small	10	
3387	FG552	0	L	sC	Sr, Dr	1.1					8	10	6	132	concentric and laminated	none or small	10	shark tooth
3388	B83	-	-	sC	Sr	1.0					3	58	250	152	concentric and laminated	brownish rock	0	shark tooth, pumice [buried]
3389	FG553	4	H	-	(Tr, Vr)	1.1			2					124	concentric layers surrounding rocks	none or small	0	basalt
3390	FG554	0	L	sC	Sr	0.7					2	25	9	77	concentric and laminated	none or small	0	
3391	FG555	0	L	-	(Vr)	tr							1	<1			0	
3392	FG556	0	L	sC	Vr, Sr	0.2					1	9	2	20			30	whale earbone
3393	FG557	0	L	sC	Sr, Vr, Fr	0.1					1	2	4	11	concentric and laminated	none or small	0	
3394	P354	-	-	sC		-								0				
3395	FG558	0	H	cO		0.0								0				
3396	FG559	0	H	cO		0.0								0				
3397	FG560	0	H	cO	Fs.r, Sr	0.3				1	0	0	1	37	laminated layers surrounding broken nodules	none or small	0	
3398	FG561	20	H	sC	ISs, IDs, Fs	5.6				9	8			0	dense layers surrounding broken nodule	brownish rock	20	
3399	B84	10	M	sC	IDPs, IDs	11.8			1	21	93	1	1	1796	dense layers surrounding broken nodule	brownish rock	70	[exposed]
	B84X	-	-	-	IDPs, IDs	>3.8				9	18			580	dense layers surrounding broken nodule	brownish rock	40	[-16 cm depth]
3400	P355	-	-	sC	IDs	-					1			24	concentric and laminated	zeolitic rock	0	[1 buried nod; -715 cm]
3401	C19	-	-	-		-								0				
3402	FG562	2	-	scO	ISs, IDs	1.2					13			140	concentric and laminated	zeolitic rock	10	
3403	D514	-	-	-	SPs.r, Ss.r	-								520kg				shark tooth, pumice

STA=station no.; SAM=sample no.; COV=sea-floor coverage (%);

SED (column 1)=sediment consistency: H= hard, M= medium, L=loose;

SED (column 2)=sediment type: s=siliceous, c=calcareous, p=pelagic, O=ooze, C=clay;

NOD-TYPE=morphological type: S=spherical, D=discoidal, P=polynucleated, I=irregular, T=tabular, F=fragmented or faceted, V=variable for shape and s=smooth, r=rough, s.r=intermediate for surface structure;

ABD=nodule abundance (kg/m^2): tr=less than 0.05 kg/m^2, $-$=no available data, ( )=doubtful data;

Size distribution: Numbers above column=diameter fraction in cm (e.g., 8 means the fraction from 8 to 10 cm in diameter), numbers of nodules shown on table;

WT= total weight of nodules collected; INTERNAL=internal structure;

POLY=number % of poly-nucleated nodules; REM=associated rocks collected;

POSITION= occurrece and depths of nodules on/in sediment column.

REGIONAL SURVEY

3246 FG424

0.0 kg/m² 0 % -

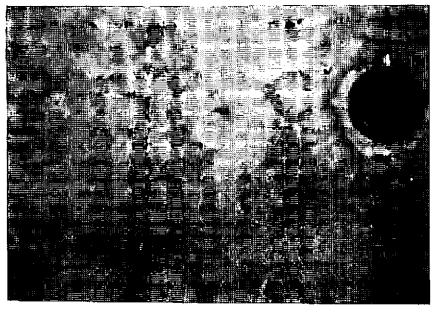

3248 FG426-1

4.0 kg/m² 1 % IDs,Fs,Is

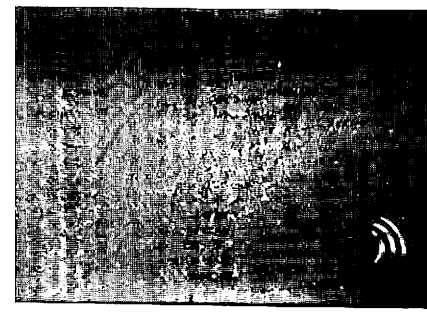

3247 FG425

16.0 kg/m² - SPs,ISPs,Ts

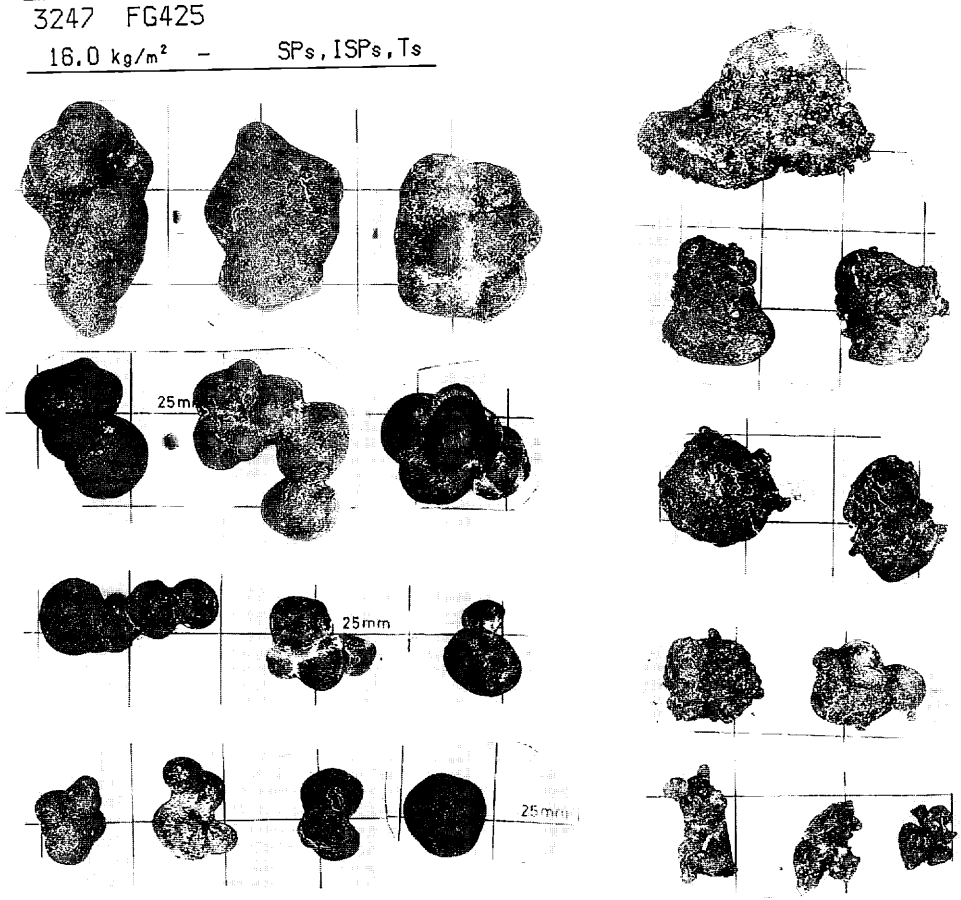

Appendix X-2 Sea-bed occurrence and morphology of manganese nodules. Each title includes station and sample numbers (in first row) and abundance, sea-floor coverage, and morphological type (in second row). Data with ( ) may be doubtful. Diameter of trigger weight in sea-bed photos is approximately 10 cm. Scale mesh and bar with nodule samples: 25 mm. Width of box core surface: 40 cm.

3248 FG426-2

3.4 kg/m² 1 % IDs, Is

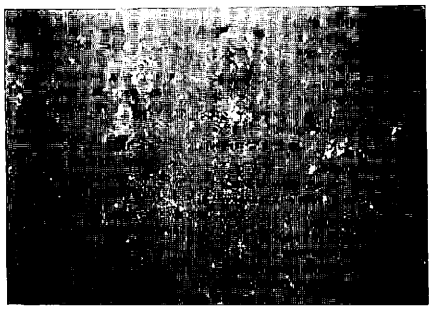

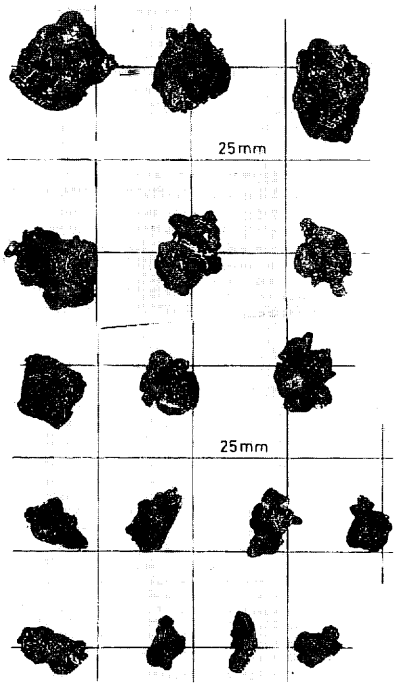

3248 P336

– – IDs

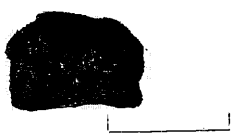

3249 FG427

0.0 kg/m² 0 % DPs

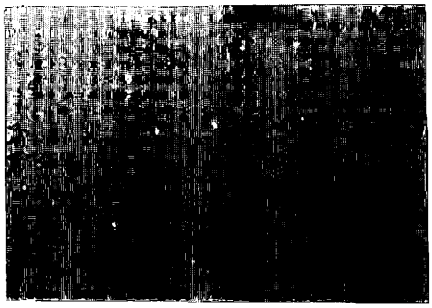

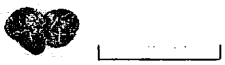

3251 FG428

5.7 kg/m² – IDs, IDPs, Ts, Fs

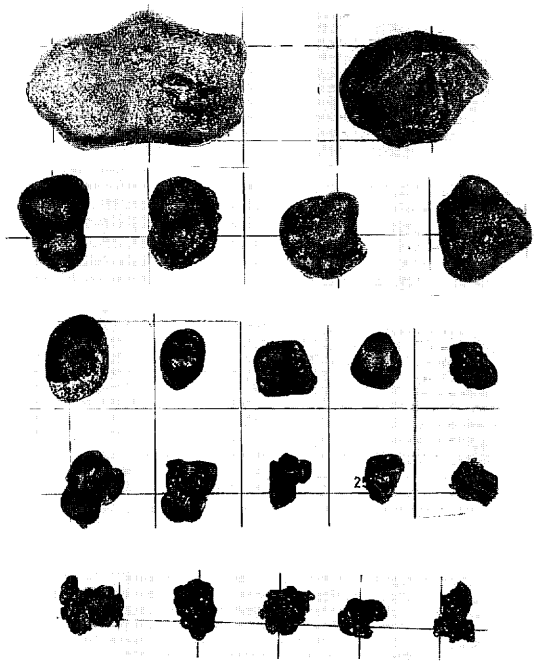

Appendix X-2 (continued)

3252 FG429

0.0 kg/m² - -

3254 FG431

0.4 kg/m² 1 % IDs,DPs

3253 FG430

0.0 kg/m² 0 % Vs

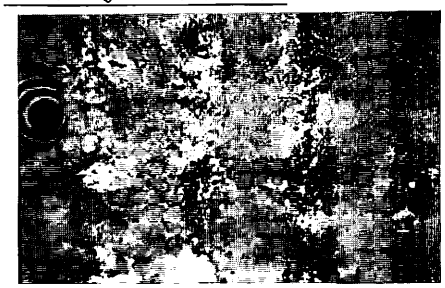

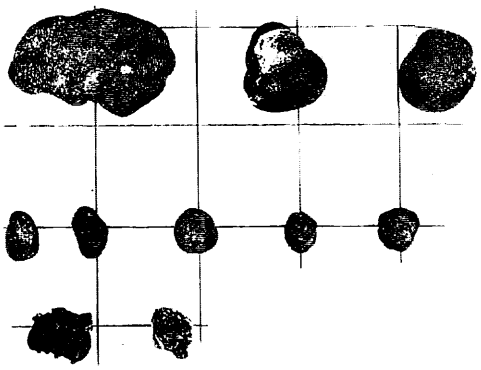

3253 B71

0.0 kg/m² 0 % Vs

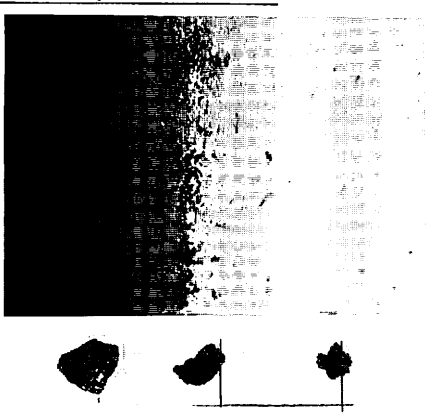

3255 FG432

0.0 kg/m² 0 % -

3256 FG433

0.0 kg/m² - -

Appendix X-2 (continued)

3257 FG434

0.0 kg/m² 0 % –

3259 FG436

0.0 kg/m² – –

3258 FG435

1.5 kg/m² – IDs, DPs

3260 FG437

0.0 kg/m² 0 % (Sr)

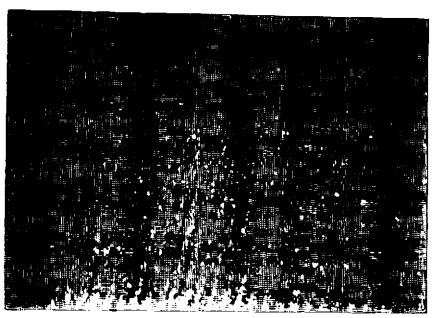

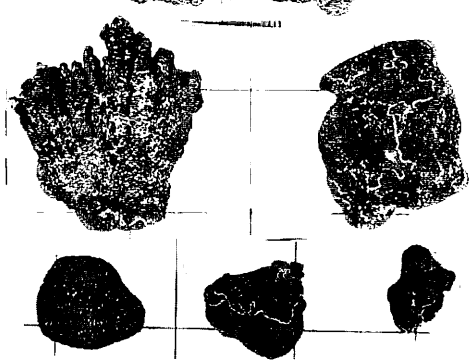

3261 FG438

0.0 kg/m² 0 % –

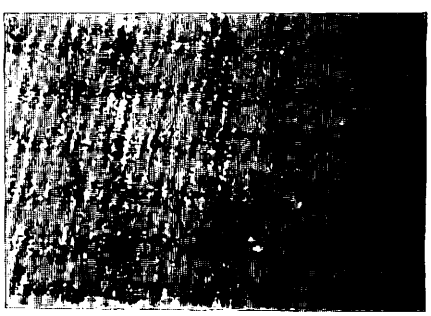

Appendix X-2 (continued)

3262 FG439

0.0 kg/m² - -

3262 P337

- - IDsr

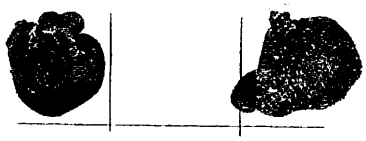

3263 FG440

0.0 kg/m² 0 % -

3264 FG441

0.0 kg/m² 0 % -

3265 FG442

0.0 kg/m² 0 % (Sr)

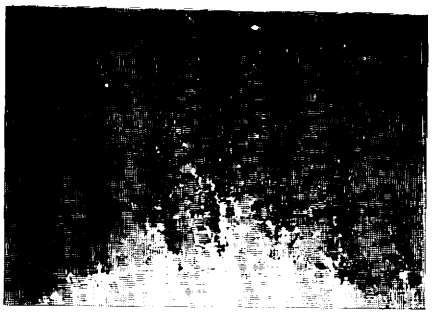

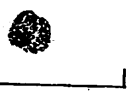

3265 P338

- - -

3266 FG443

0.0 kg/m² 0 % -

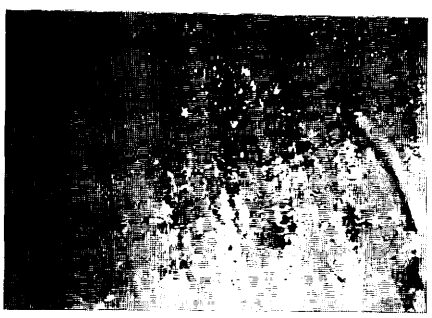

Appendix X-2 (continued)

3267 FG444

15.8 kg/m² 15 % IDs,IDPs,Ts,Fs

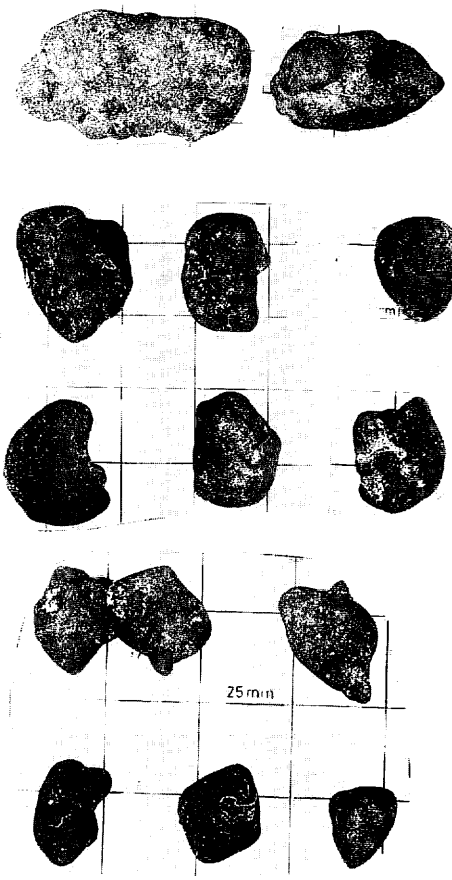

3268 FG445

0.4 kg/m² 0 % Ds,IDPs,Fs

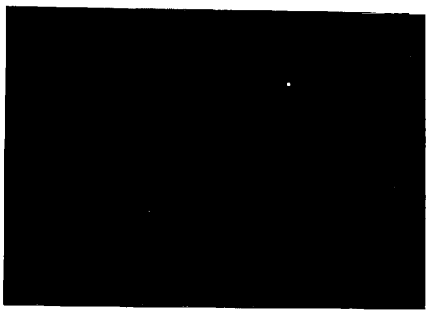

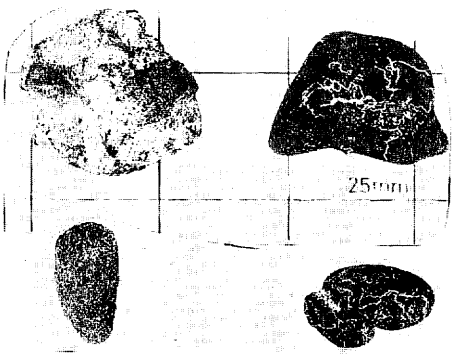

3269 FG446

0.0 kg/m² 0 % -

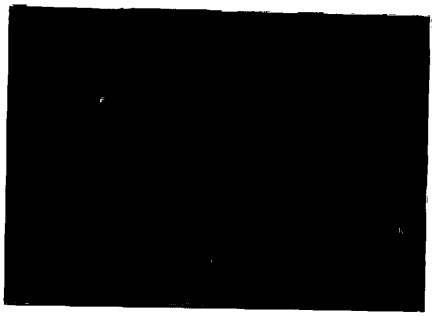

3270 FG447

0.0 kg/m² - -

Appendix X-2 (continued)

3271 FG448

0.0 kg/m² 0 % –

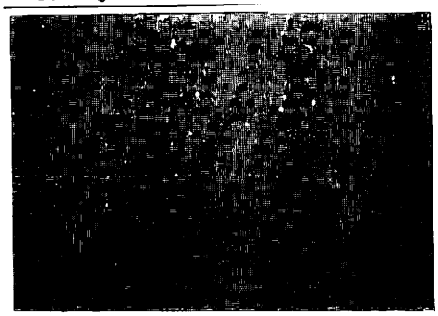

3272 FG449

0.0 kg/m² 0 % –

3271 B72

0.0 kg/m² 0 % –

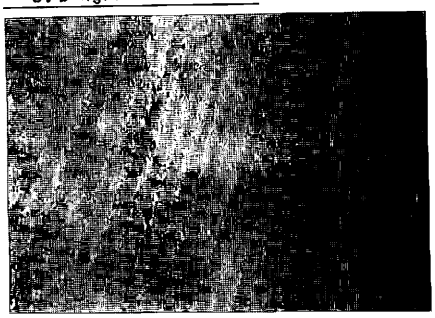

3273 FG450

0.0 kg/m² 0 % –

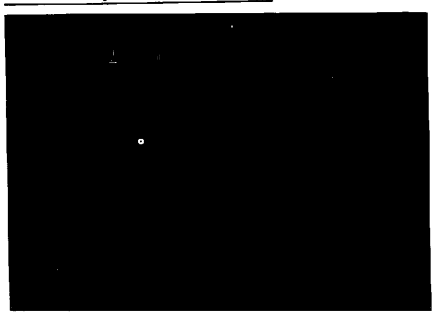

box core surface

3274 FG451

0.0 kg/m² 0 % (Ir)

Appendix X-2 (continued)

3275 FG452

2.3 kg/m² 1 % IDs, Ts, Is

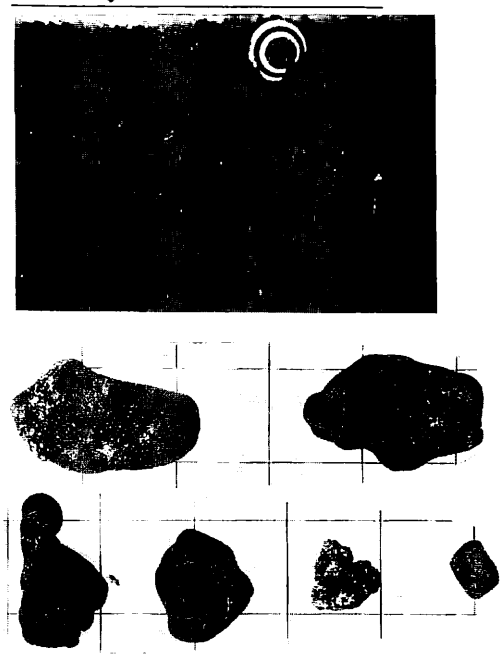

3276 FG453

0.1 kg/m² 0 % Ir, Sr

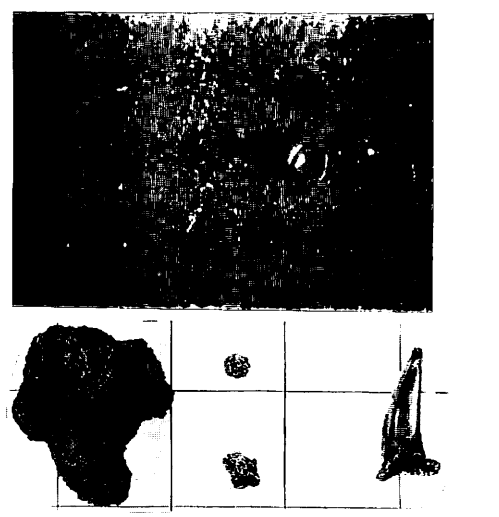

3277 FG454

3.5 kg/m² - Sr

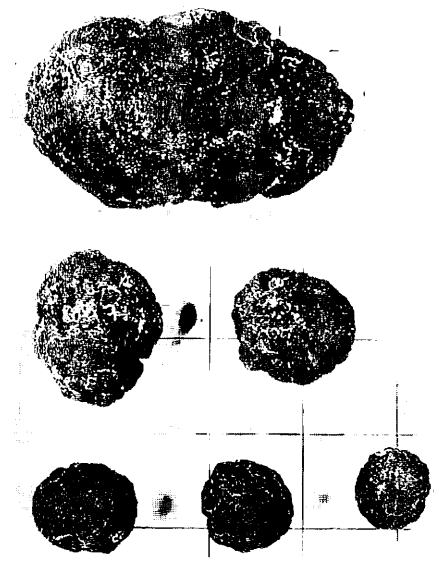

3277 P339

- - -

3278 FG455

0.1 kg/m² - Sr

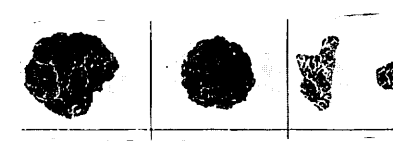

Appendix X-2 (continued)

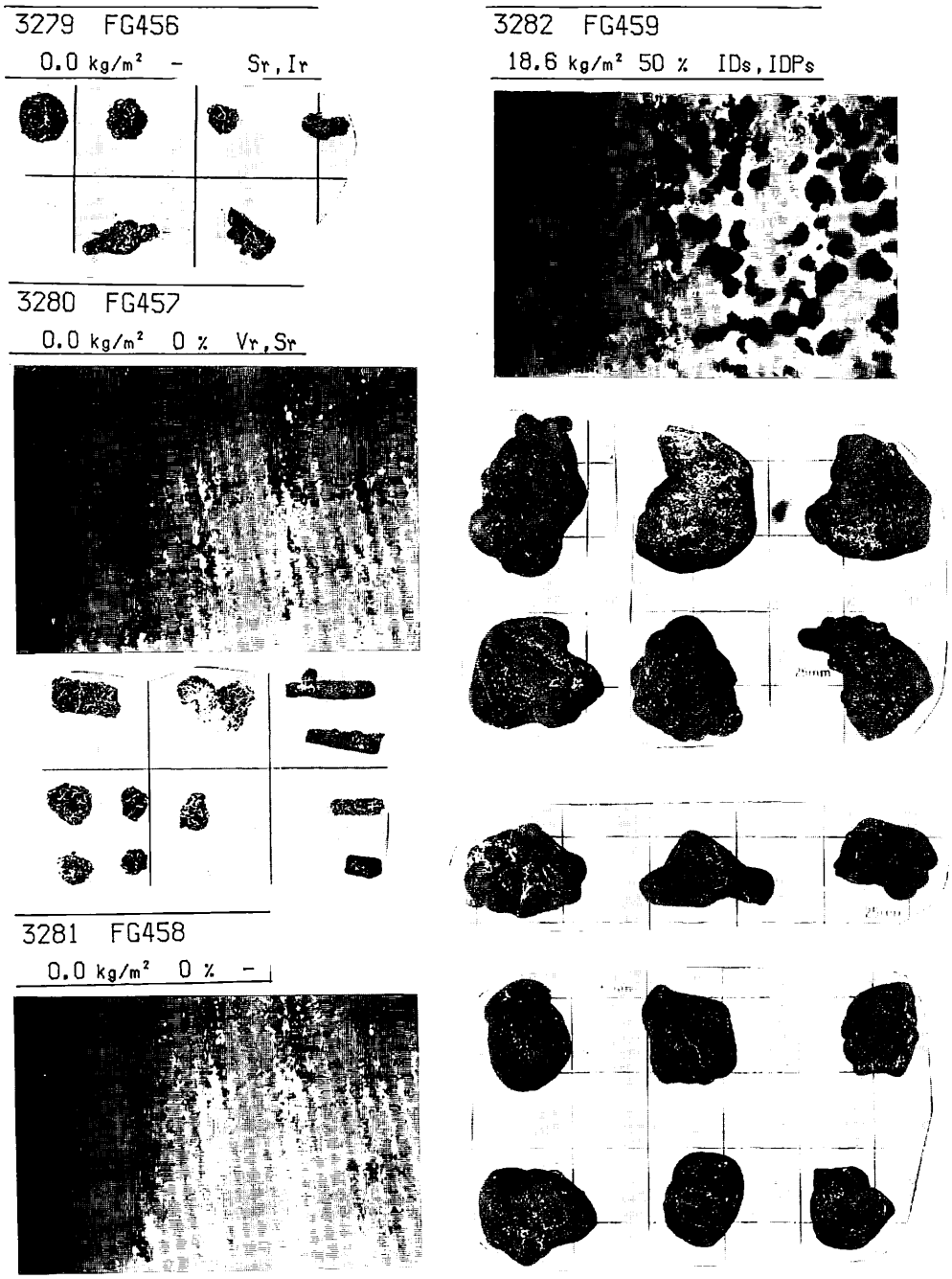

Appendix X-2 (continued)

3283 FG460

0.0 kg/m² 0 % Sr, Vr

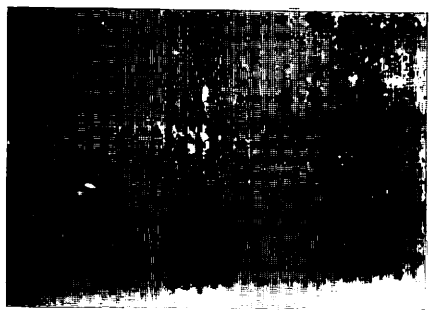

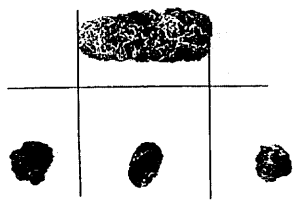

3283 B73

0.0 kg/m² 0 % Vr

box core surface

Appendix X-2 (continued)

3284 FG461

9.3 kg/m² 3 % IDs-r, DPs-r

3285 FG462

0.0 kg/m² - -

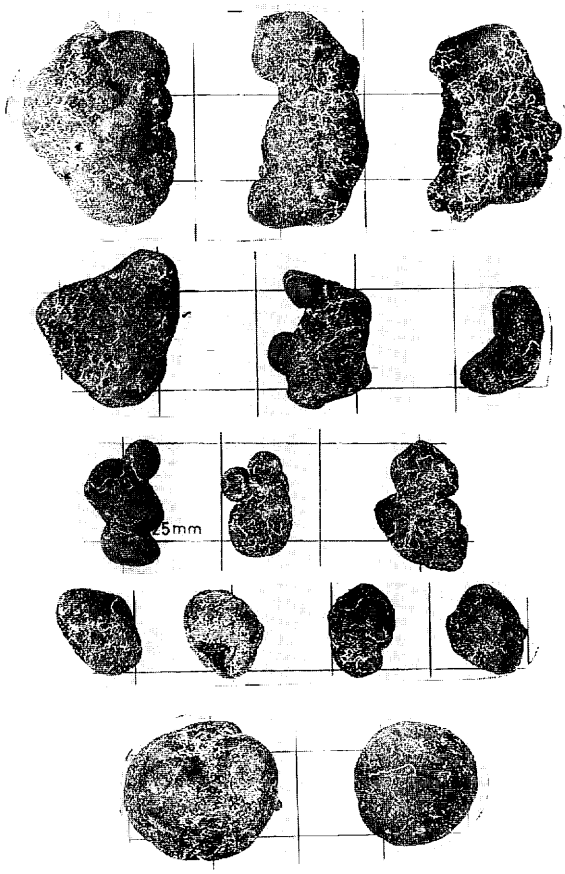

3286 FG463

0.0 kg/m² 0 % -

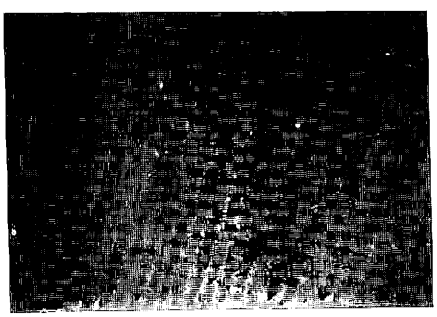

Appendix X-2 (continued)

3287 FG464

19.8 kg/m² 30 % IDPs,DPs

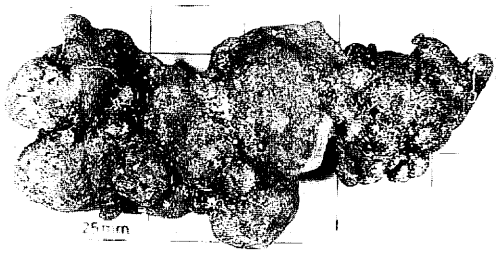

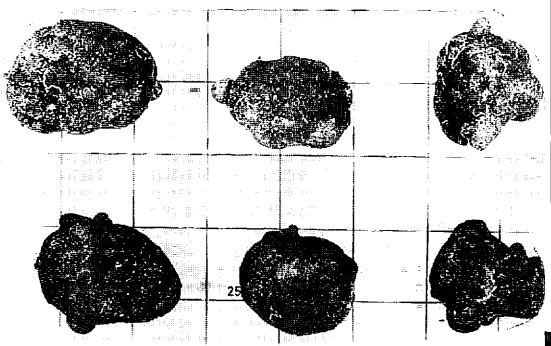

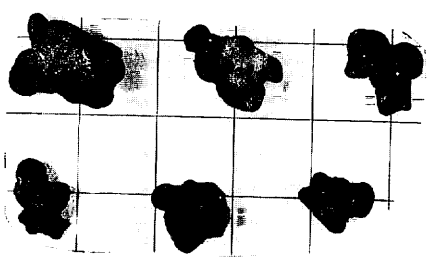

3288 FG465

0.0 kg/m² 0 % -

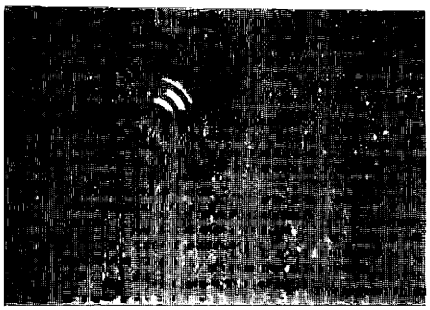

3288 P340

- - -

3289 FG466

0.0 kg/m² 0 % -

3290 FG467

0.0 kg/m² 0 % -

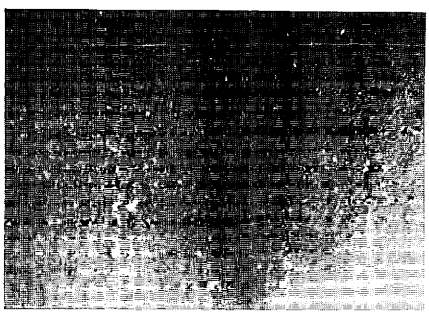

Appendix X-2 (continued)

3291 FG468

0.0 kg/m² 0 % –

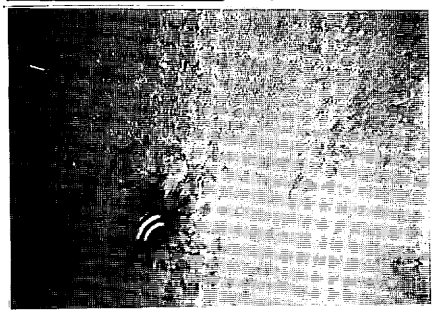

3294 FG471

0.0 kg/m² 0 % –

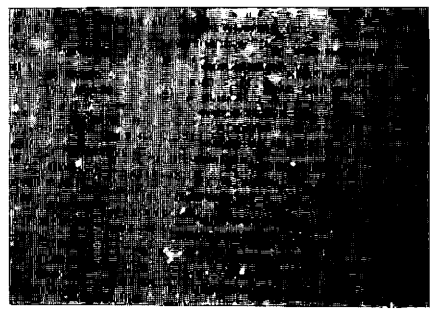

3292 FG469

0.0 kg/m² 0 % –

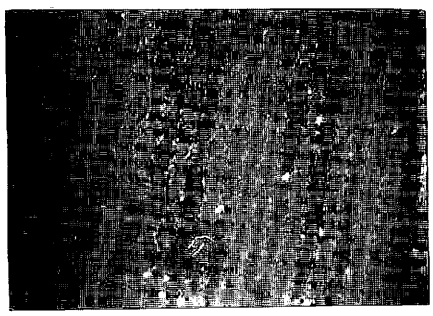

3295 FG472

0.4 kg/m² 0 % Sr

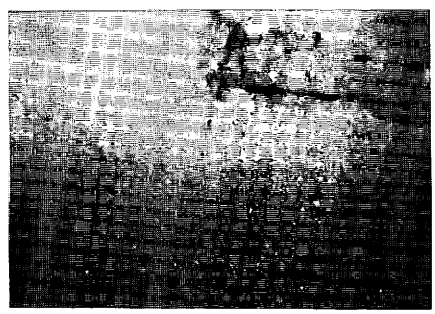

3293 FG470

0.0 kg/m² 0 % –

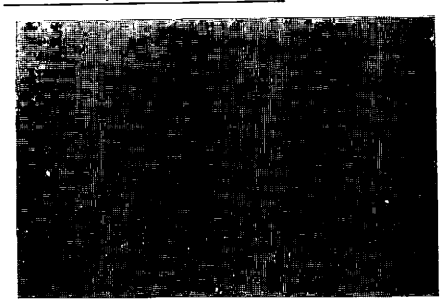

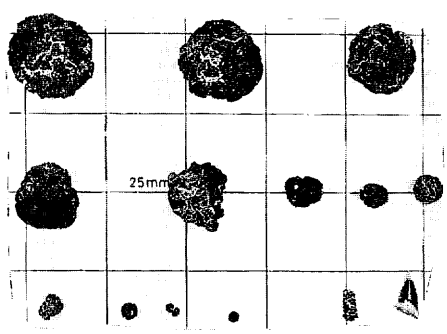

Appendix X–2 (continued)

DETAILED SURVEY

3296 FG473

0.0 kg/m² 0 % –

3298 FG475

0.0 kg/m² 0 % –

3297 FG474

2.9 kg/m² 0 % Sr

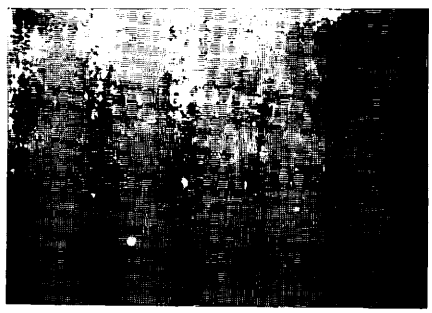

3299 FG476

7.1 kg/m² 0 % Ss·r

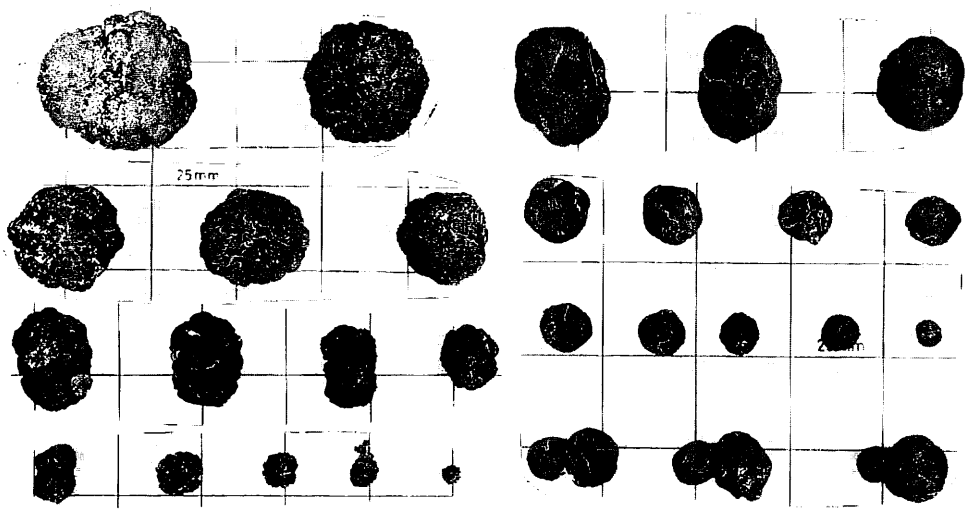

Appendix X-2 (continued)

3300 FG477

8.7 kg/m² 10 % SPs

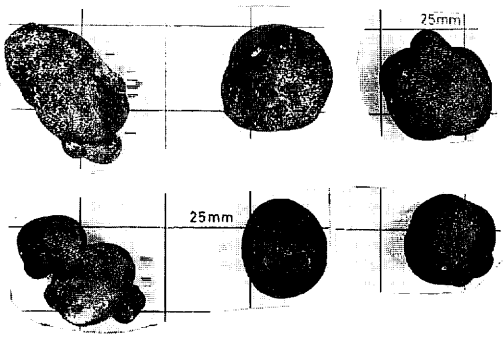

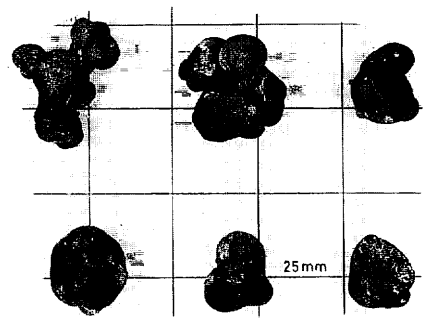

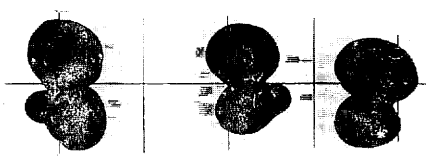

3300 B74

11.2 kg/m² 8 % SPs

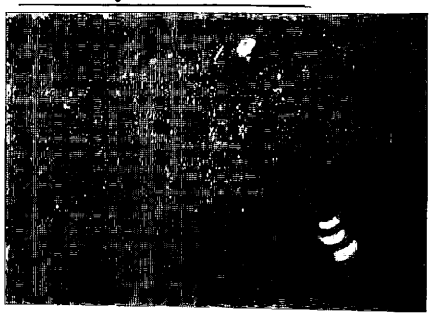

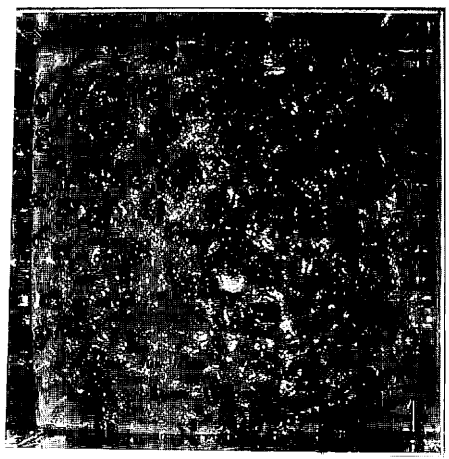

box core surface

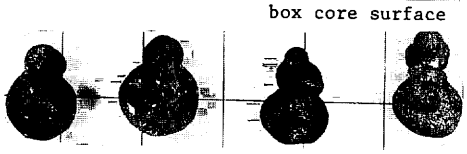

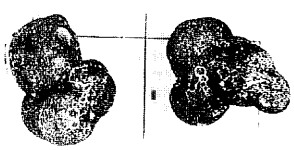

Appendix X-2 (continued)

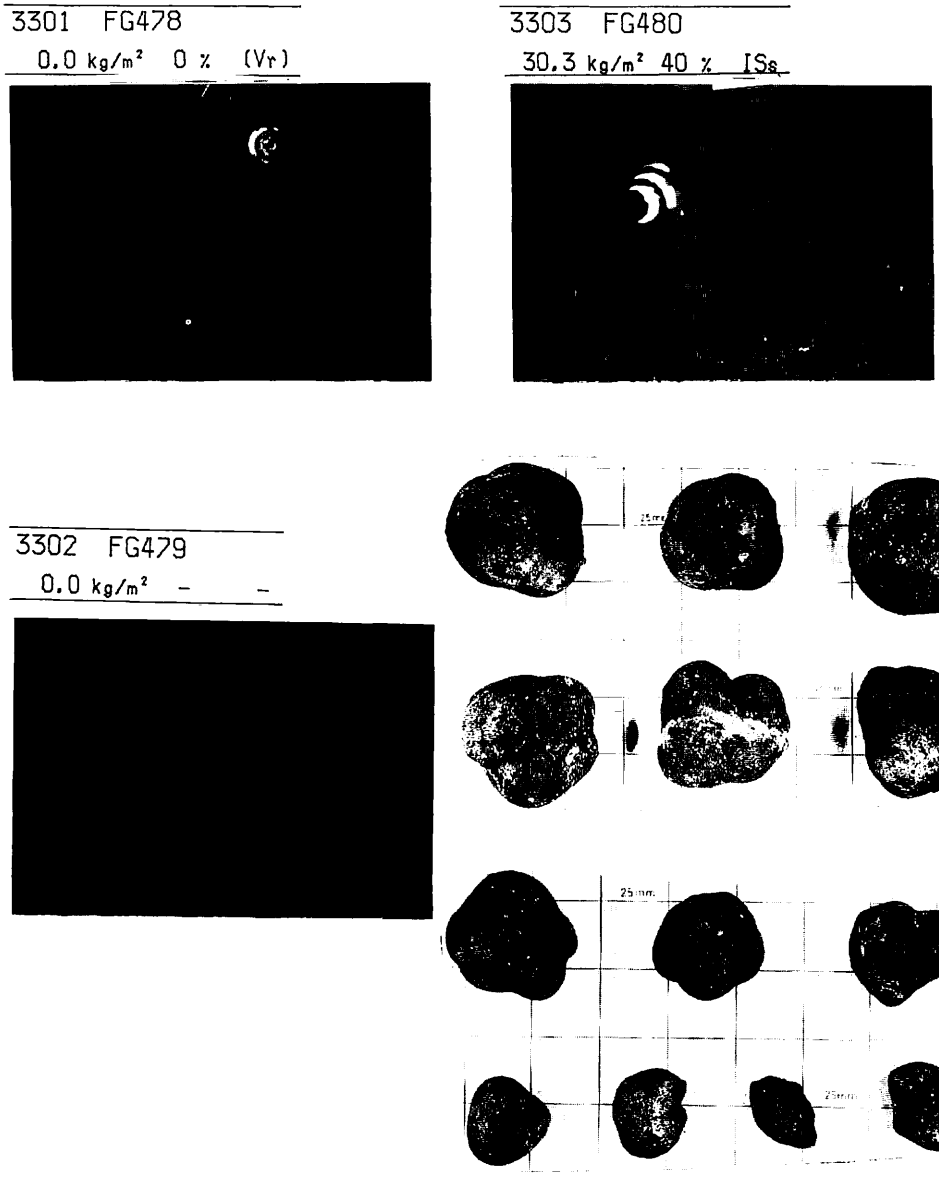

Appendix X-2 (continued)

3304 FG481

1.2 kg/m² 1 % IDs

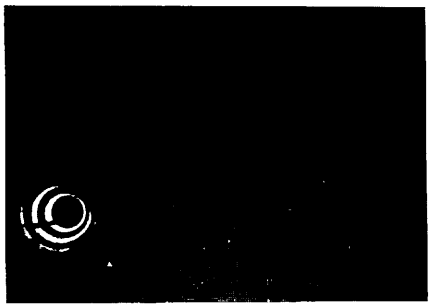

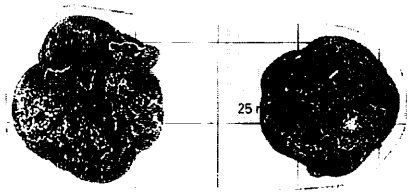

3306 FG483

11.0 kg/m² 1 % ISs, IDPs, Fs

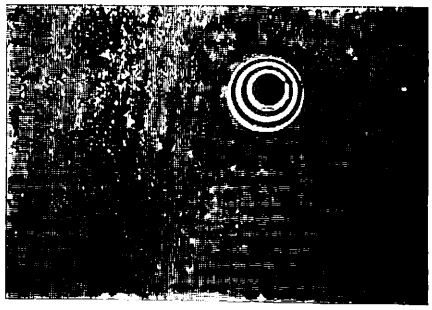

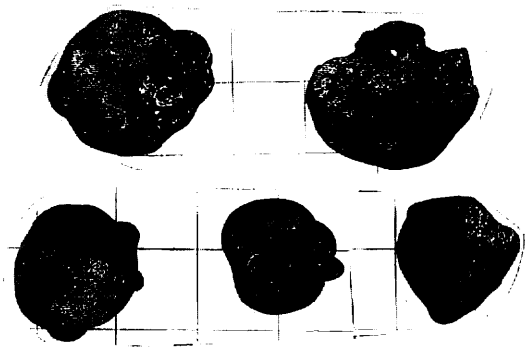

3305 FG482

0.0 kg/m² 0 % –

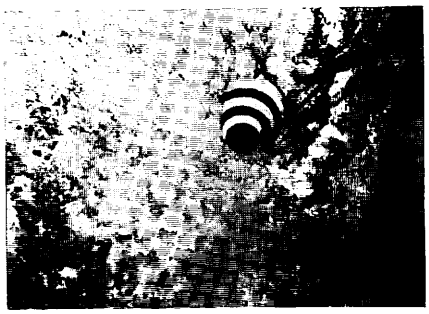

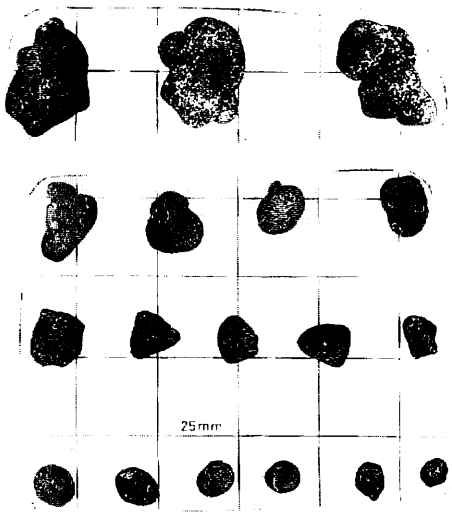

Appendix X-2 (continued)

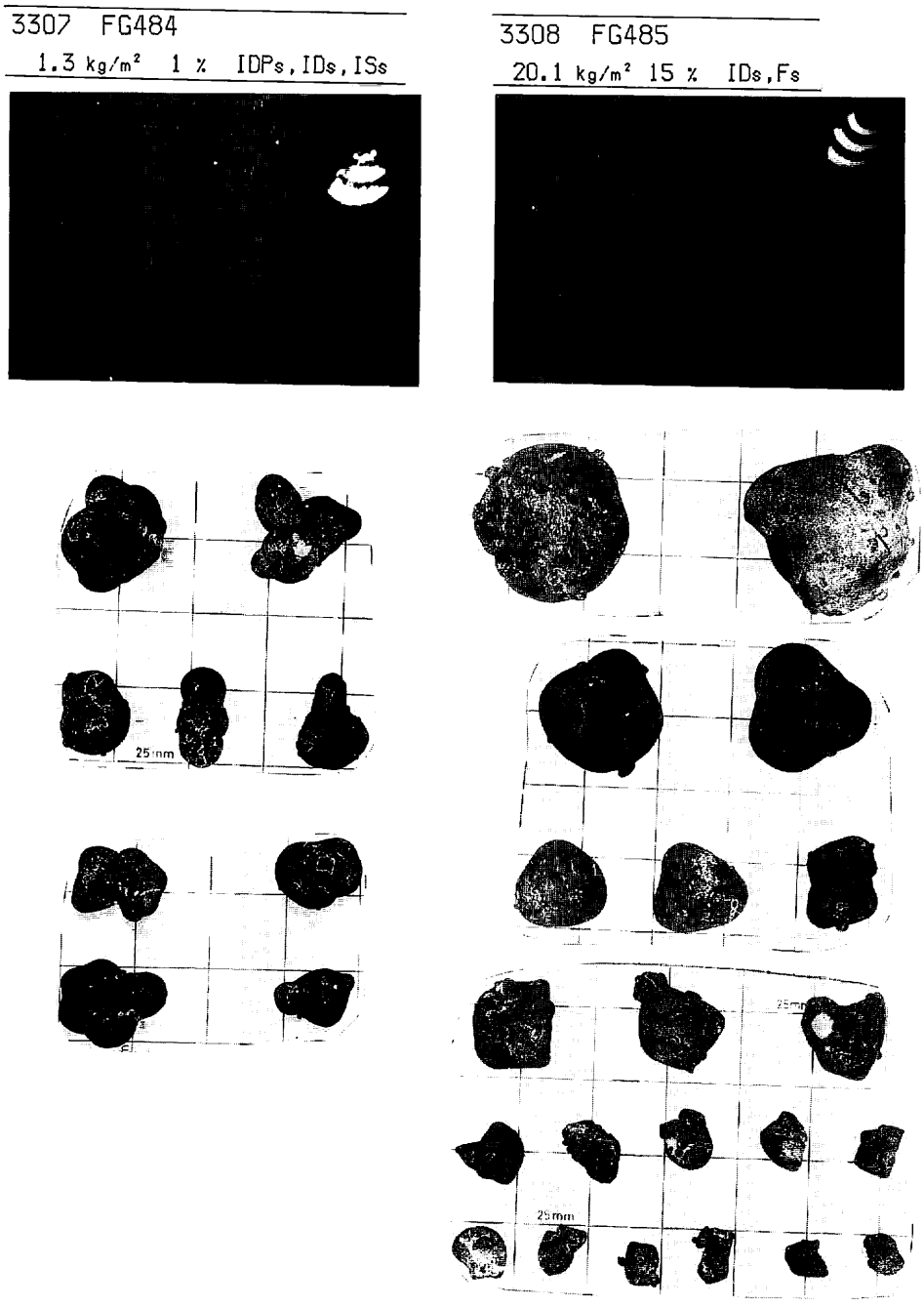

Appendix X-2 (continued)

3309 FG486

0.0 kg/m² – –

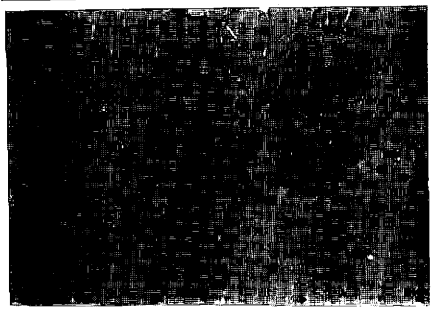

3311 FG488

20.8 kg/m² 30 % ISs, IDs

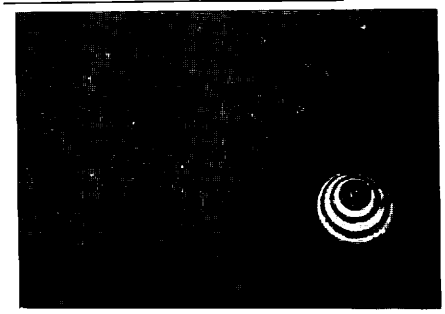

3310 FG487

6.0 kg/m² 5 % IDs, IDPs

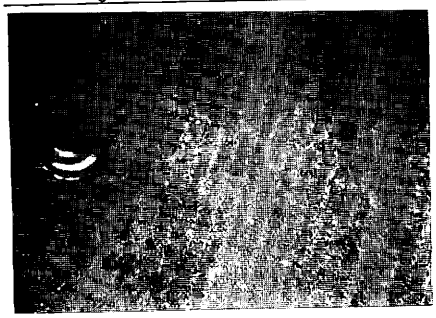

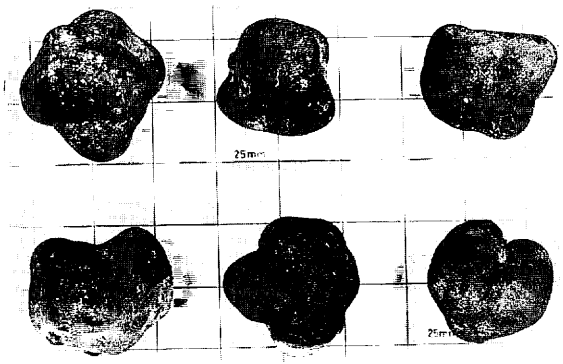

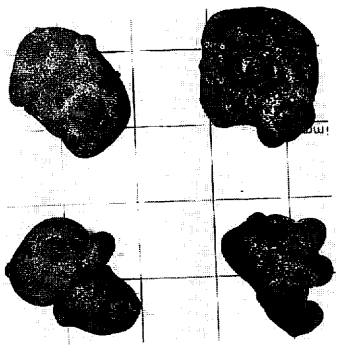

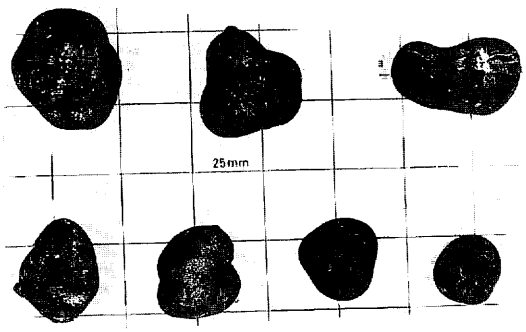

Appendix X-2 (continued)

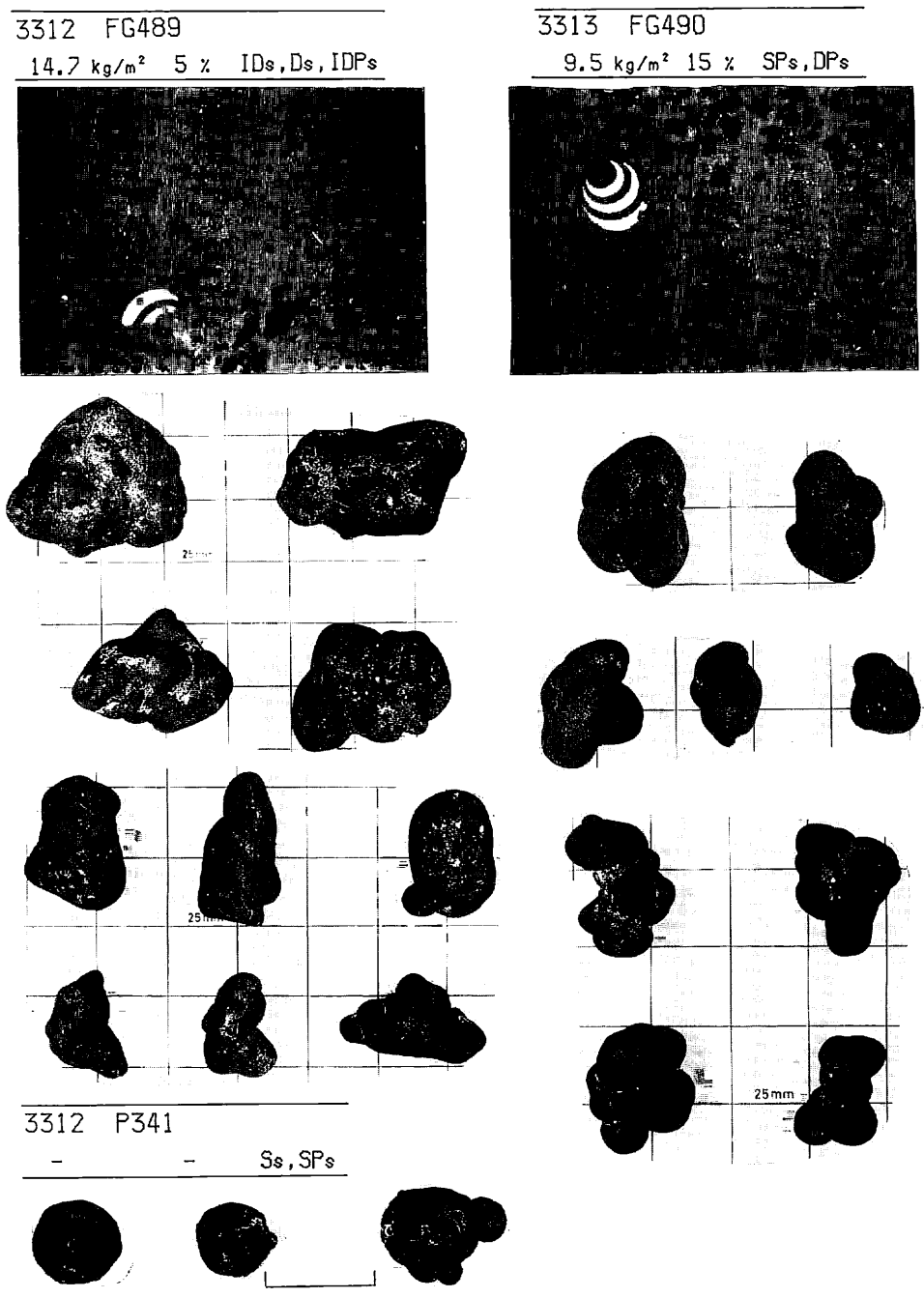

Appendix X-2 (continued)

3314 FG491

0.2 kg/m² 0 % Ss

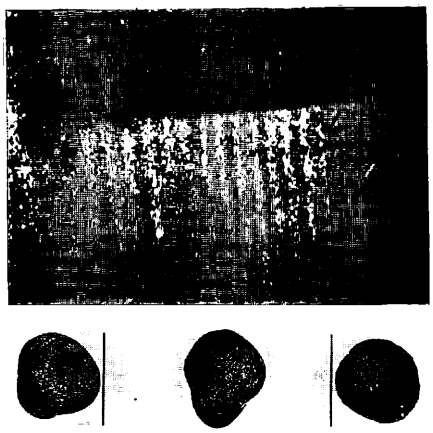

3315 FG492

5.1 kg/m² 0 % Sr

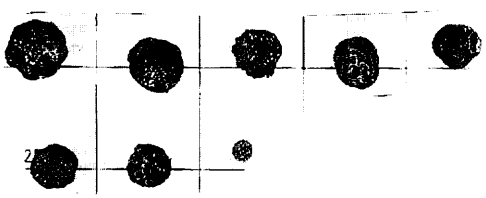

3315 P342

– – –

3316 FG493

0.2 kg/m² 0 % ISs

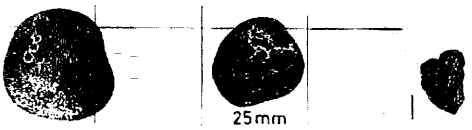

Appendix X-2 (continued)

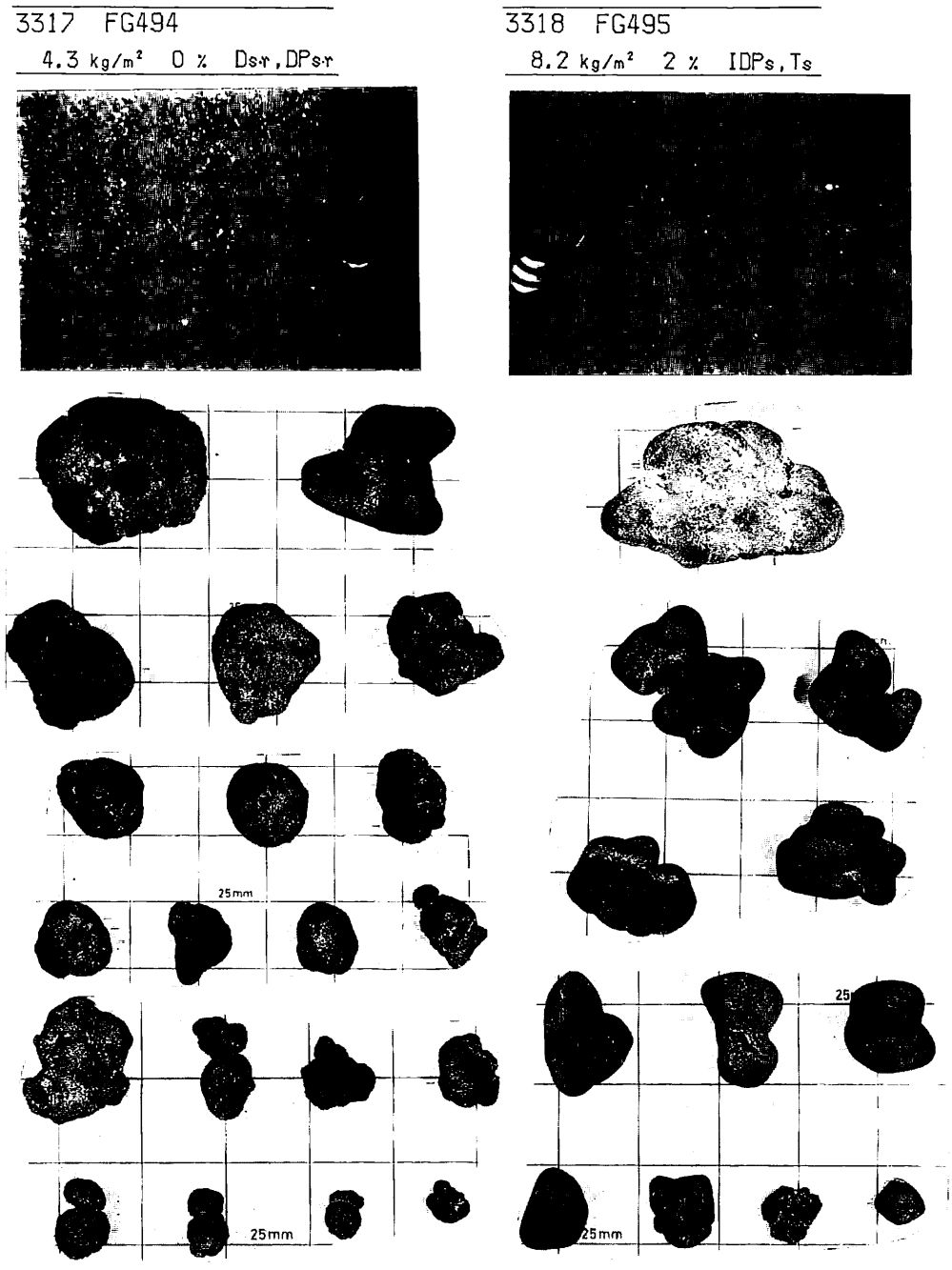

Appendix X-2 (continued)

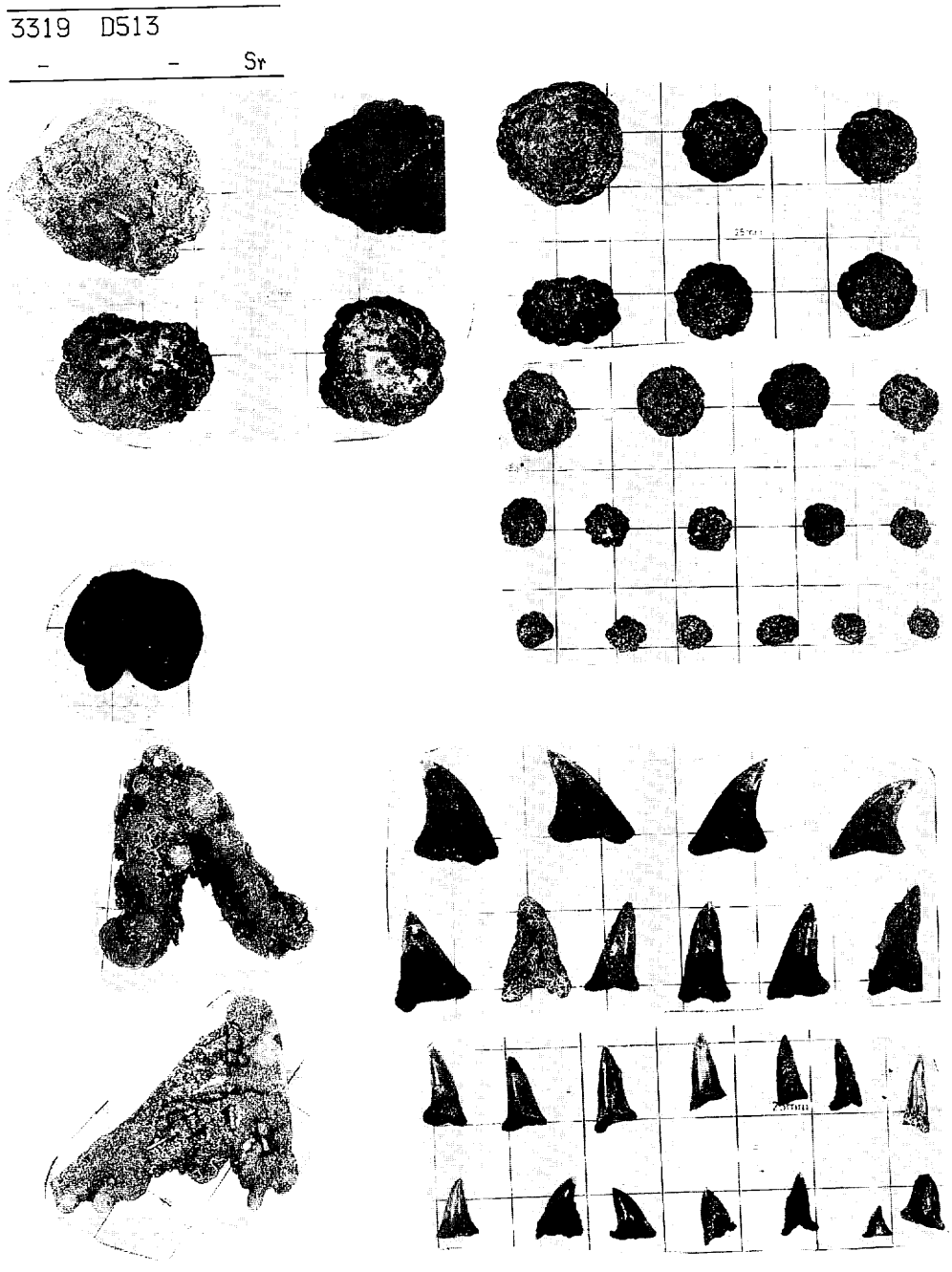

Appendix X-2 (continued)

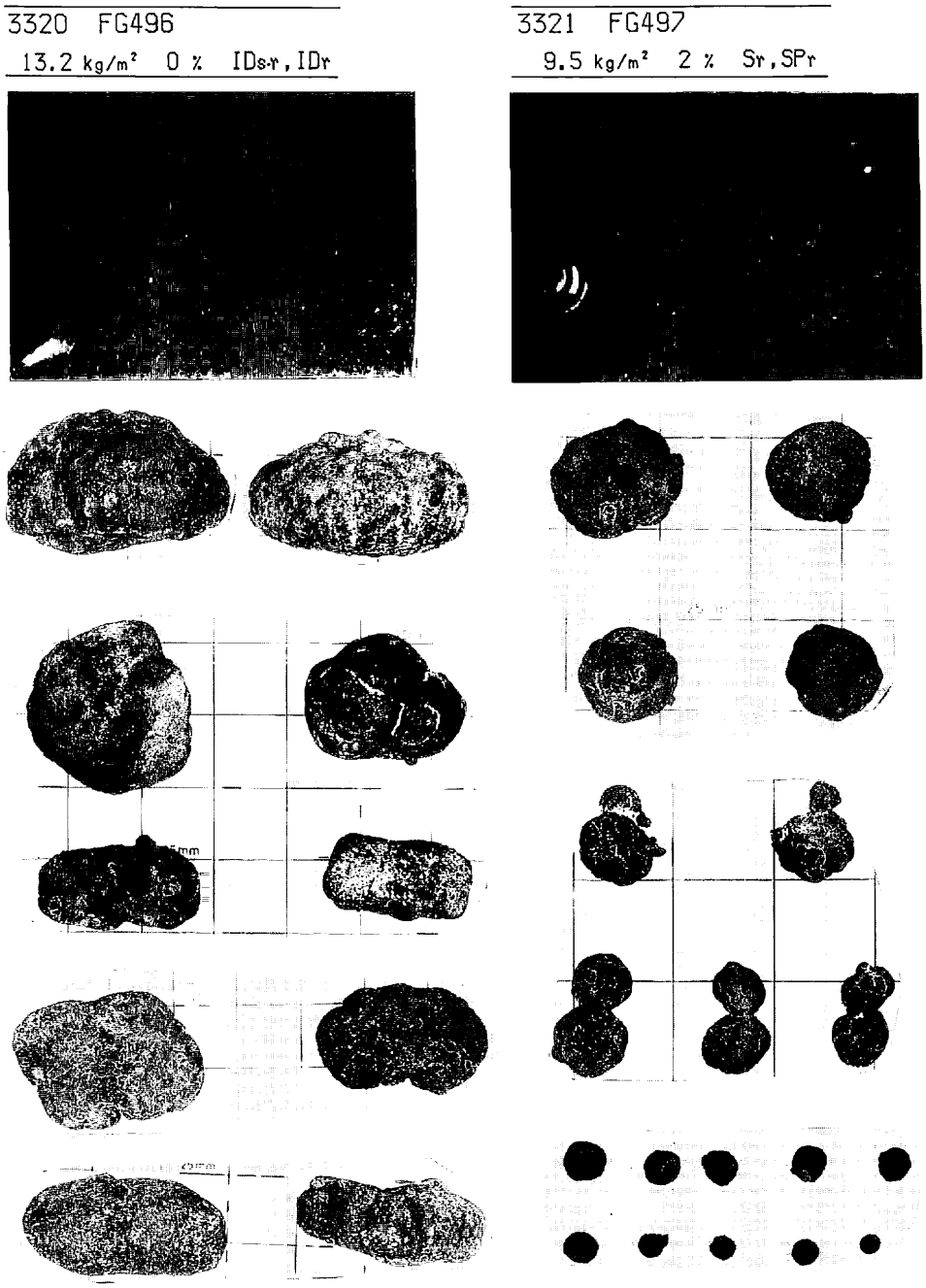

Appendix X-2 (continued)

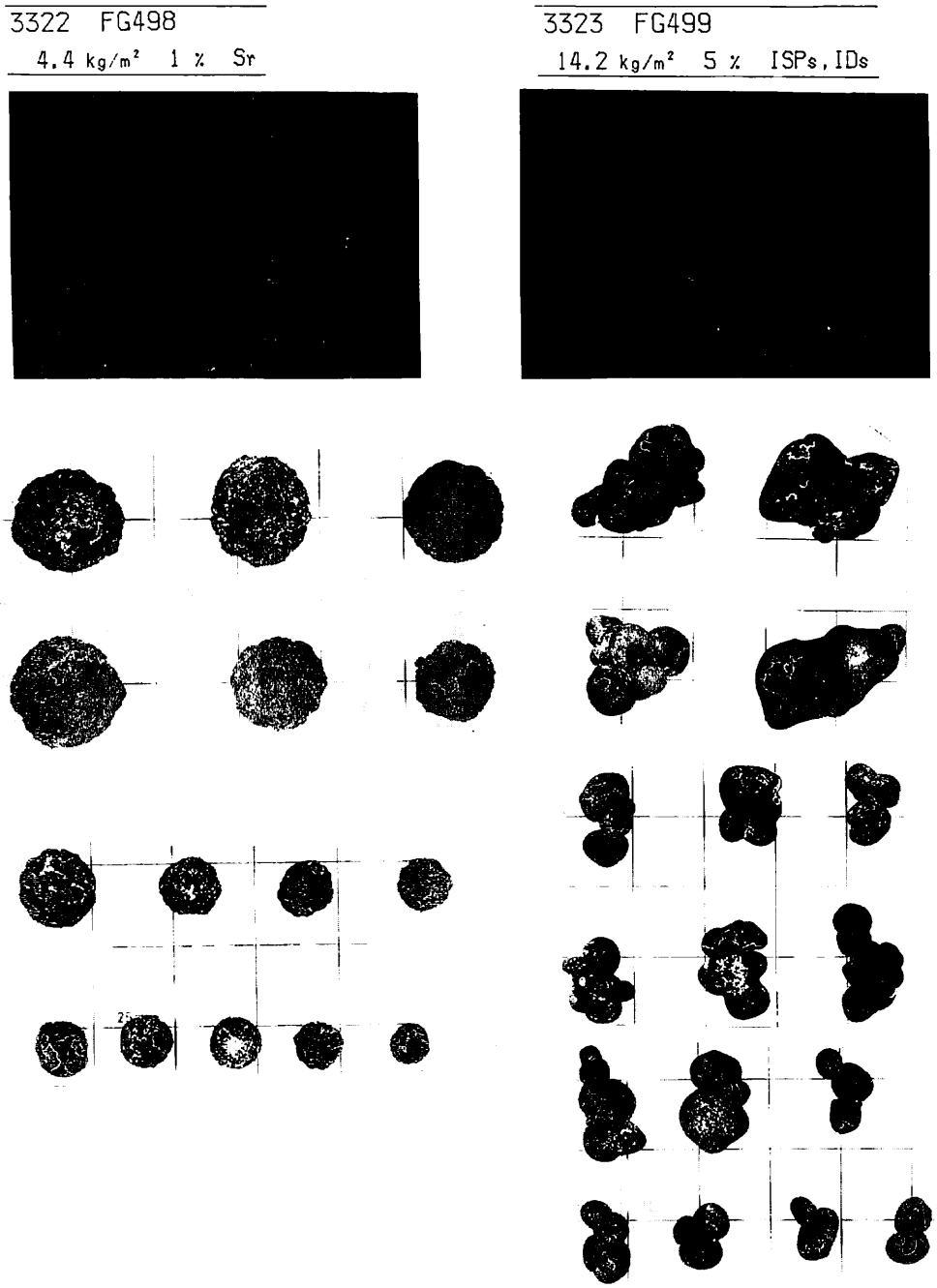

Appendix X-2 (continued)

3324 B75

6.3 kg/m² 0 % IDr, Dr, IDPr, Sr

box core surface

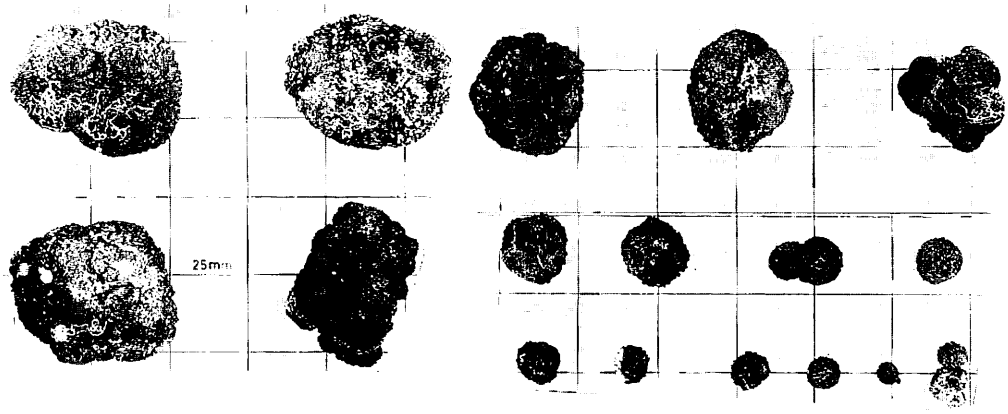

3324 B75X

– – IDr, IDPr, Dr buried at 15 cm depth

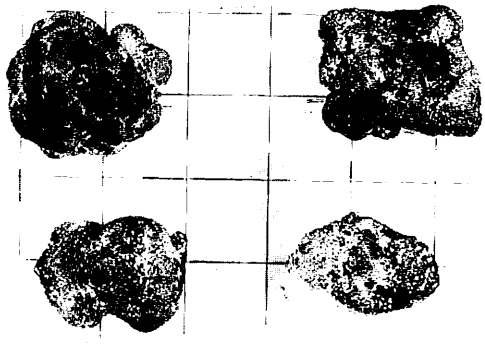

Appendix X-2 (continued)

REGIONAL SURVEY

3325 P343

– – –

3326 P344

– – –

3327 B76

0.0 kg/m² 0 % –

box core surface

3329 FG500

0.0 kg/m² 0 % –

3329 P346

– – –

3330 B77

0.0 kg/m² – –

box core surface

Appendix X-2 (continued)

3331 FG501

5.2 kg/m² 1 % IDs, IDPs

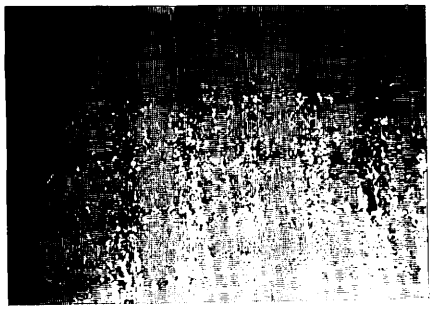

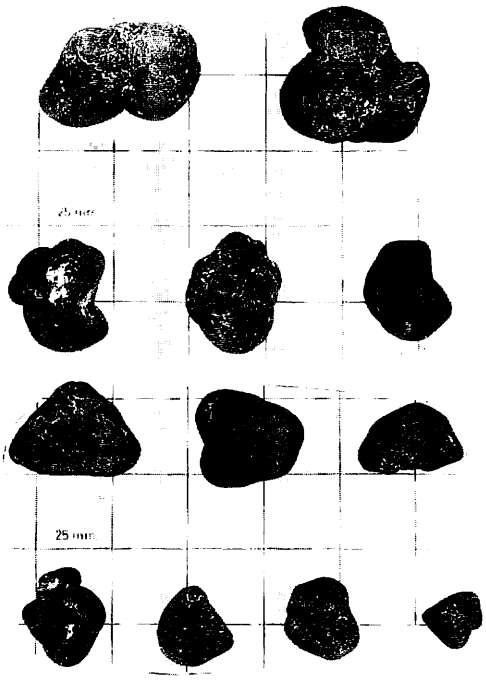

3331 P347

– – Ss, DPs

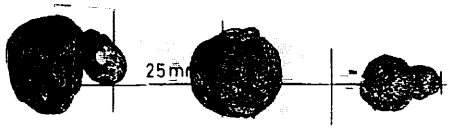

3332 FG502

0.0 kg/m² 0 % –

3332 P348

– – –

3333 B78

0.1 kg/m² 0 % Sr

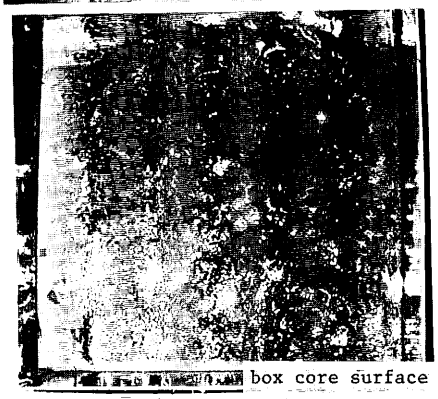

Appendix X-2 (continued)

DETAILED SURVEY

3334 FG503

13.6 kg/m² 30 % IDs, IDPs

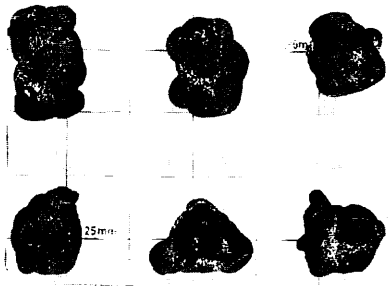

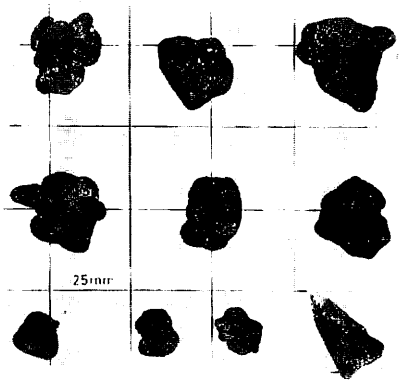

3335 FG504

1.4 kg/m² 0 % IDs·r, Sr

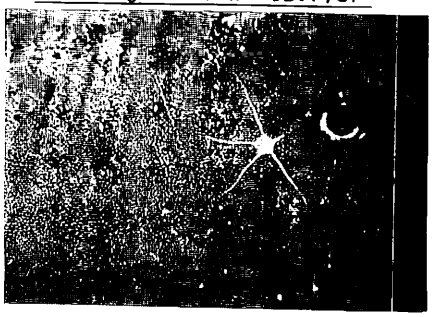

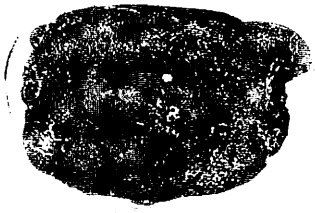

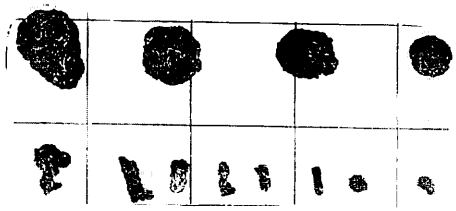

Appendix X-2 (continued)

3336 FG505

12.8 kg/m² 10 % Ss·r, SPs·r

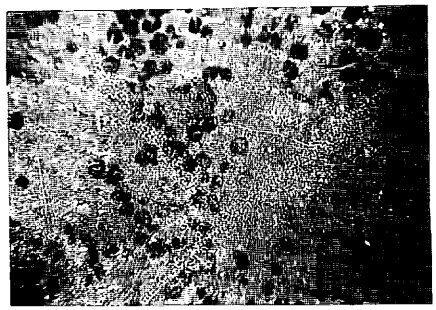

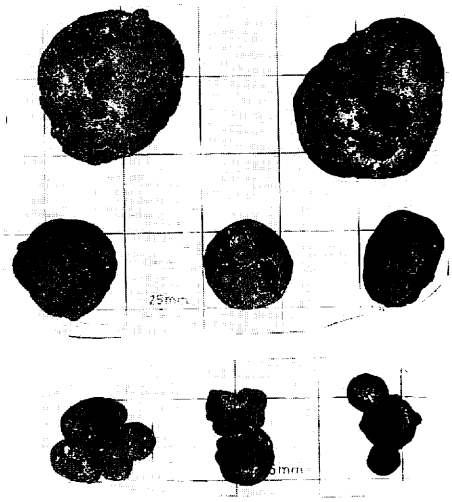

3337 FG506

6.0 kg/m² 3 % Ss·r, SPs·r

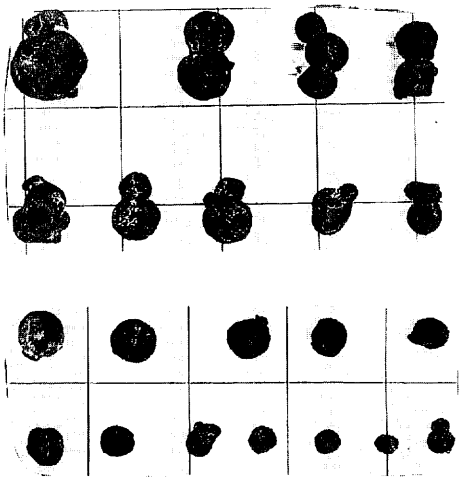

3338 FG507

0.0 kg/m² – –

3338 P349

– – SPs, ISPs

Appendix X-2 (continued)

3339 FG508

18.2 kg/m² 5 % IDPs, IDs

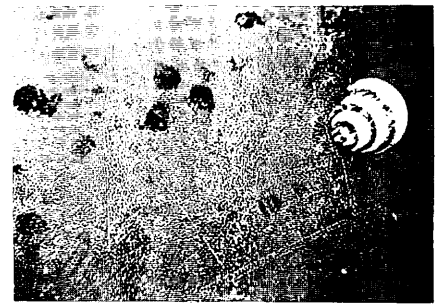

3340 FG509

16.4 kg/m² – fragments

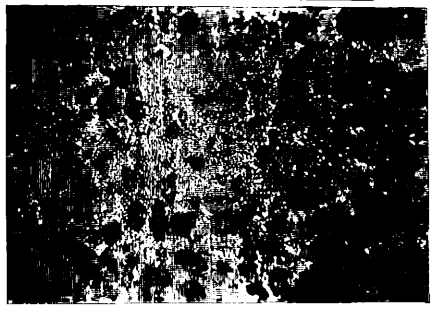

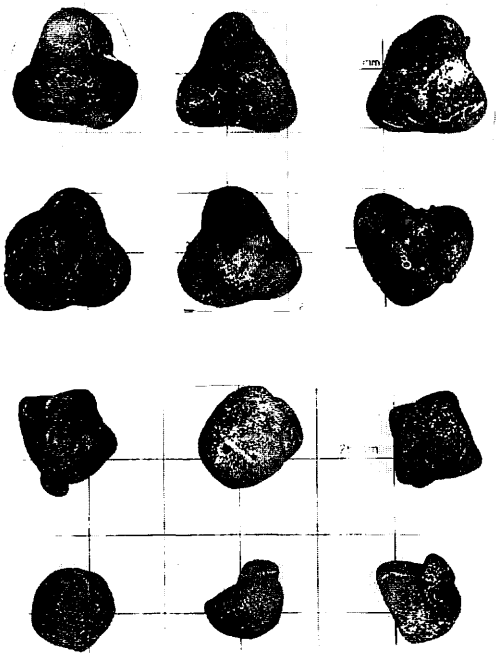

3341 FG510

12.2 kg/m² – IDs

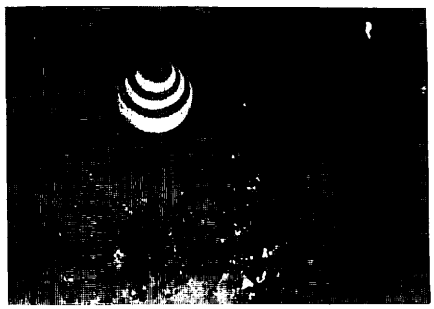

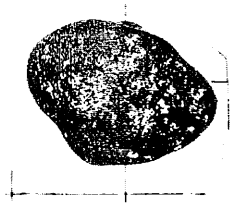

Appendix X-2 (continued)

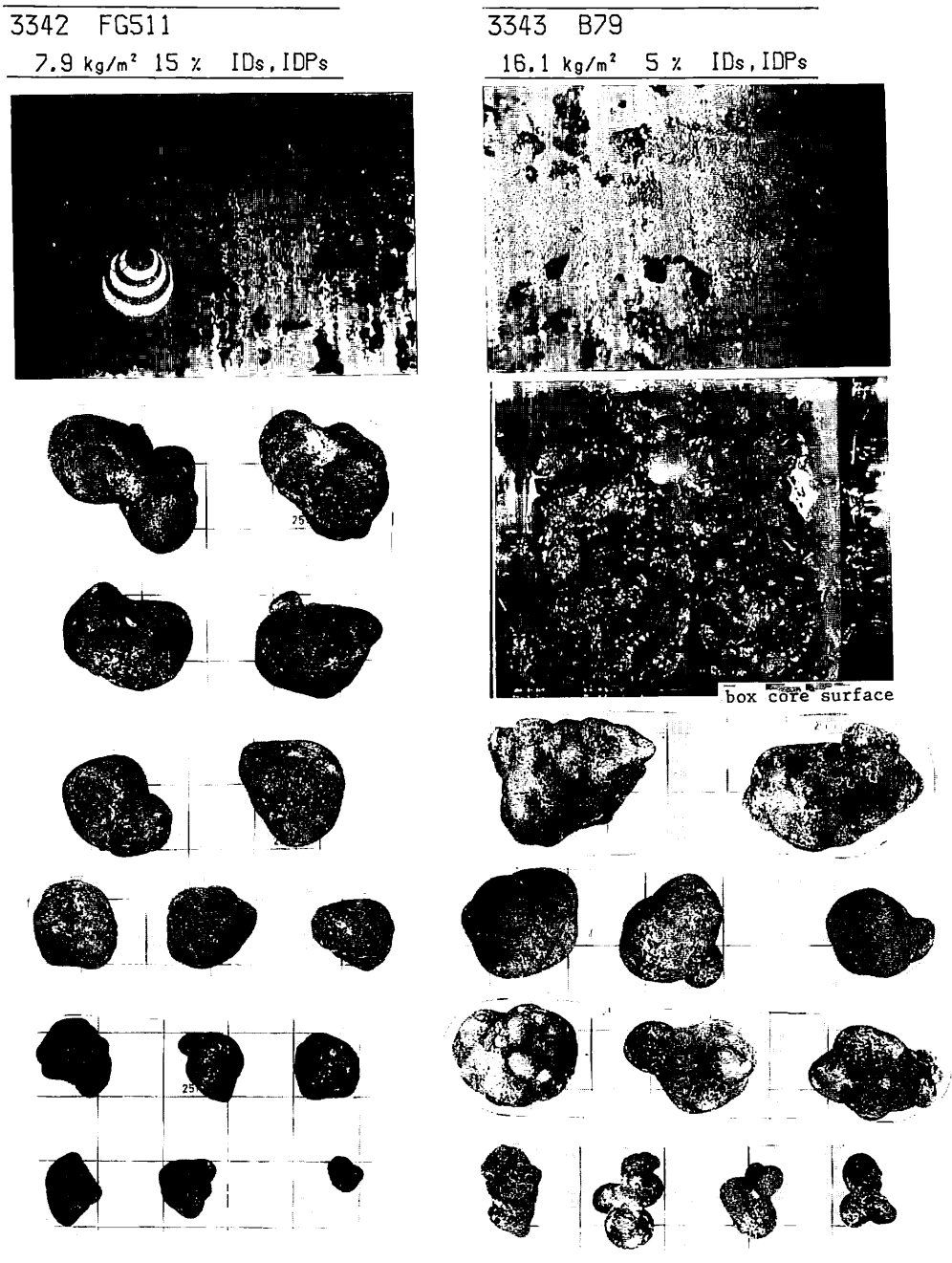

Appendix X-2 (continued)

3343 B79X

9.6 kg/m² - IDr+s

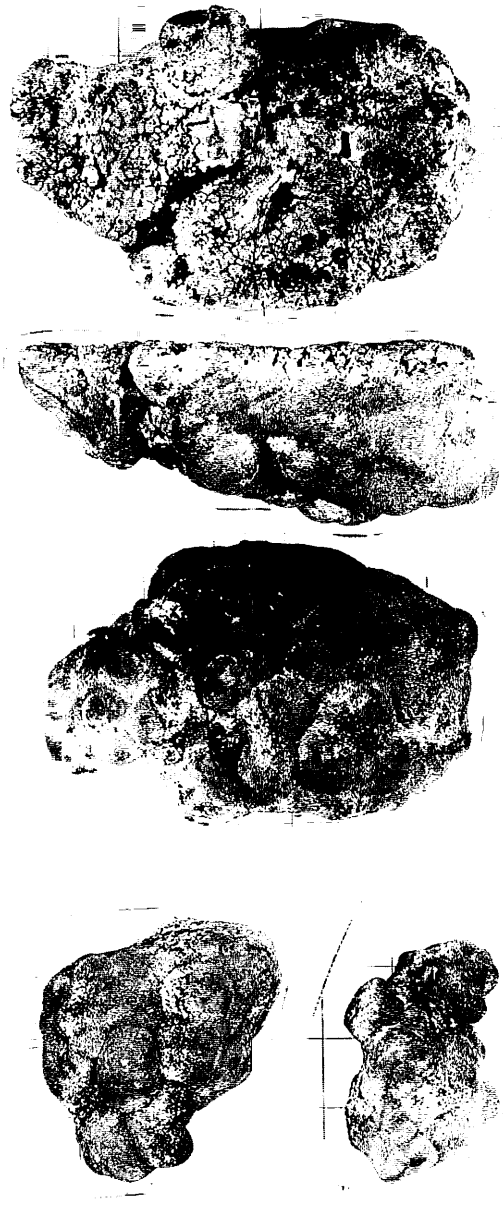

3344 FG512

7.9 kg/m² - Sr, SPr

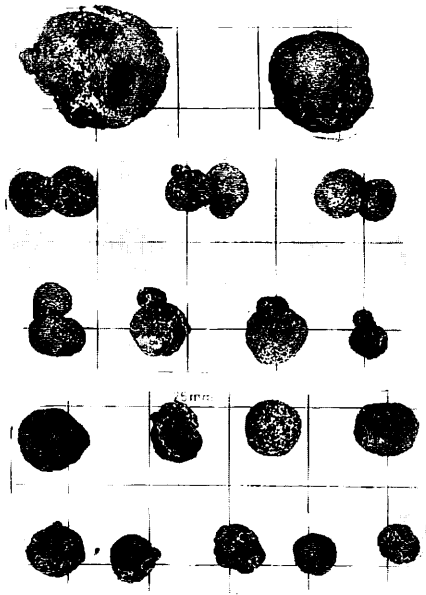

3345 FG513

16.1 kg/m² - Ssr

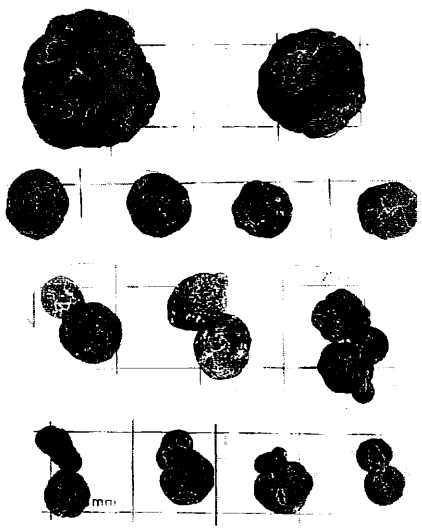

Appendix X-2 (continued)

3346 FG514

9.6 kg/m² 2 % Ss·r, SPs·r

3347 FG515

5.1 kg/m² 0 % Sr

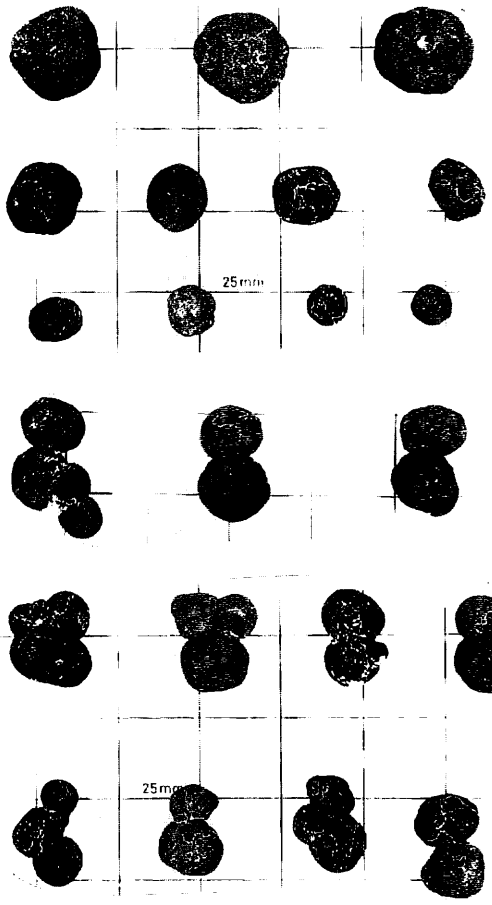

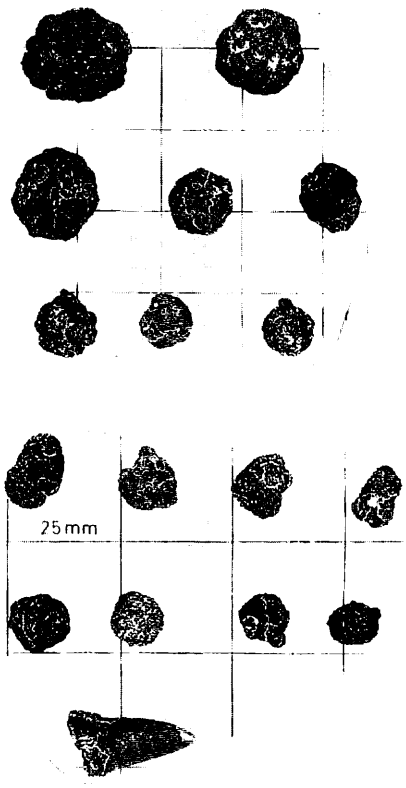

Appendix X-2 (continued)

3348 FG516

7.2 kg/m² 0 % Sr

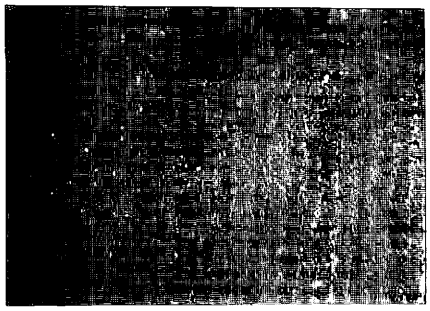

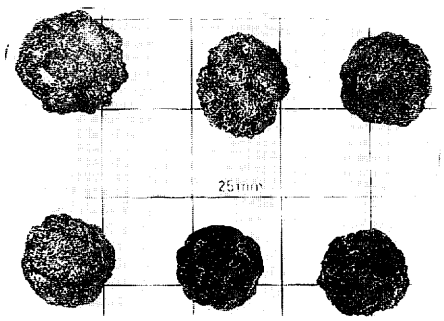

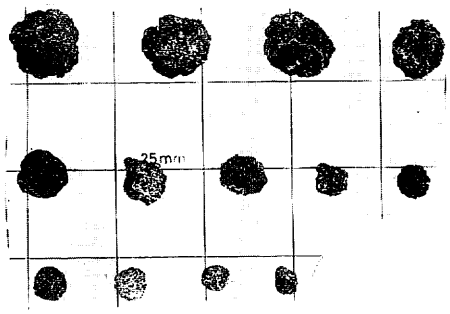

3349 FG517

0.6 kg/m² 2 % SPs·r, ISs·r

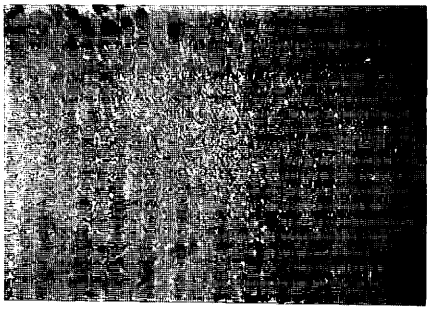

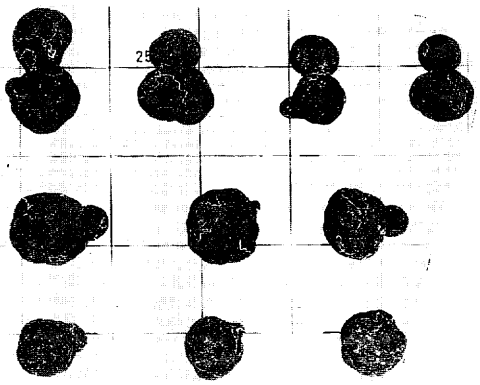

3349 P350

– – Ss·r

Appendix X-2 (continued)

3350 FG518

7.1 kg/m² 0 % SPs, Ss, ISPs

3351 FG519

2.8 kg/m² 0 % Ss·r

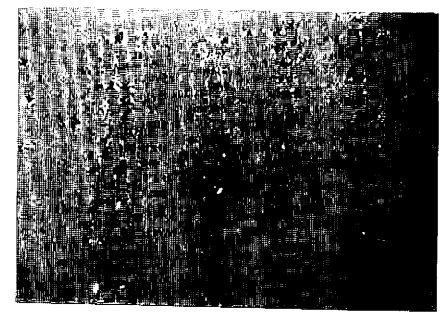

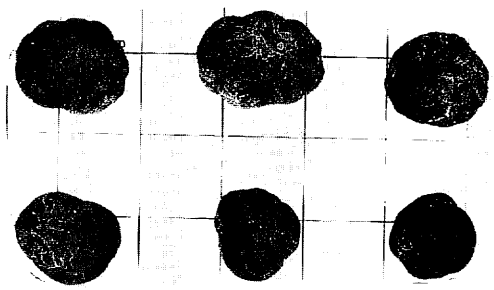

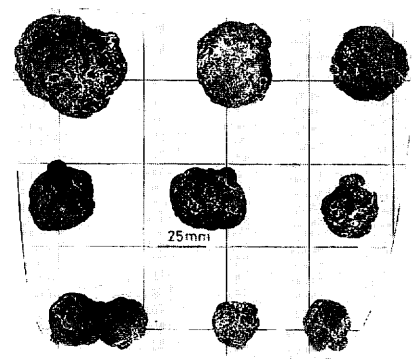

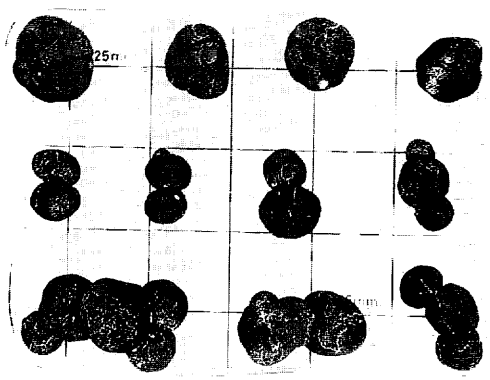

Appendix X-2 (continued)

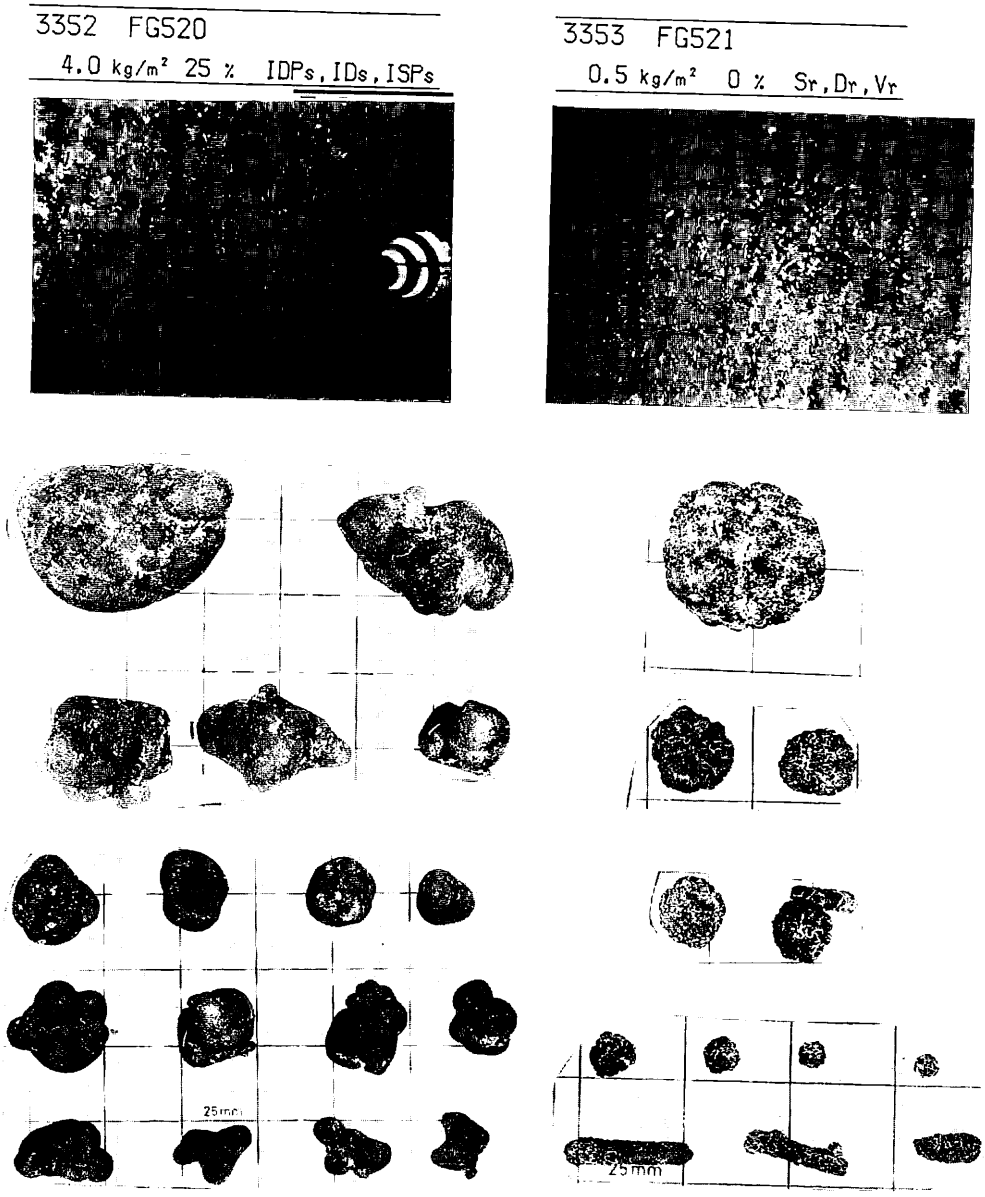

Appendix X-2 (continued)

3354 FG522

3.1 kg/m² 0 % Sr,Dr

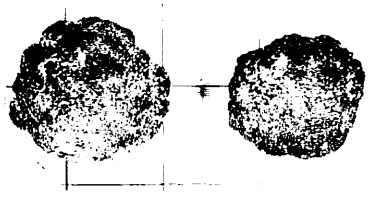

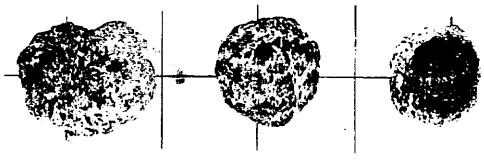

3355 B80

10.9 kg/m² – IDPs,ISPs,IDs

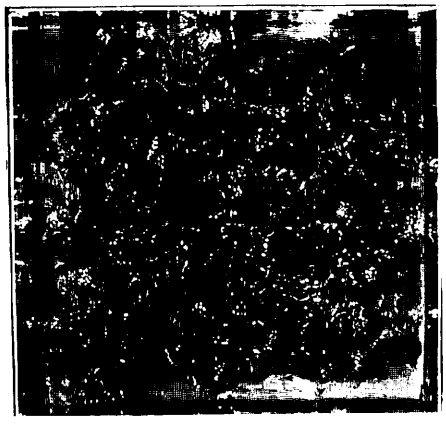

box core surface

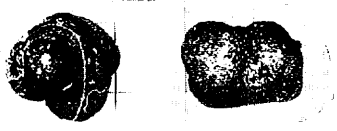

Appendix X-2 (continued)

3355 B80X

10.9 kg/m² – ISs, IDs

buried at 12 cm depth

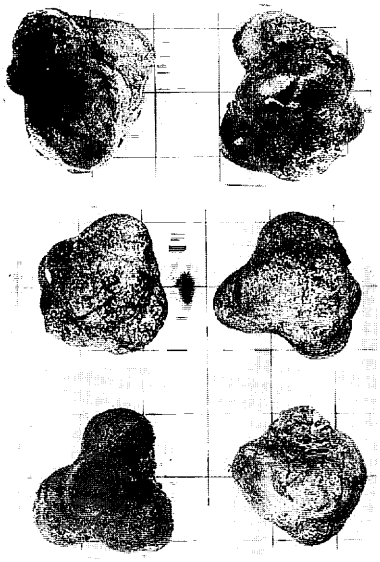

3356 FG523

0.0 kg/m² 0 % (Sr)

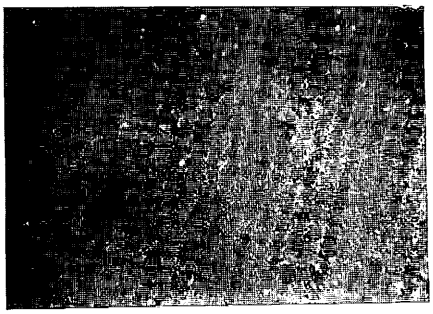

3357 FG524

14.3 kg/m² 5 % Ts, IDs, Ts+r

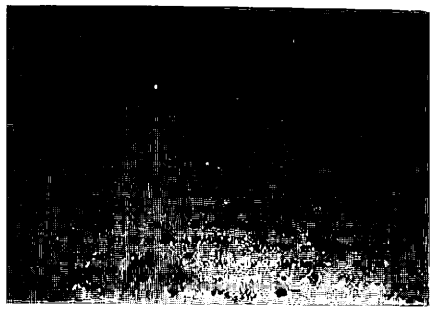

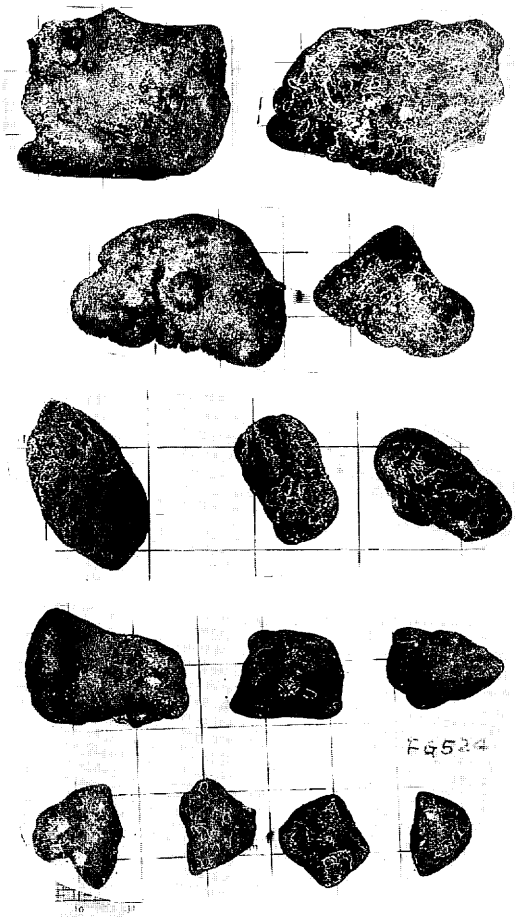

Appendix X-2 (continued)

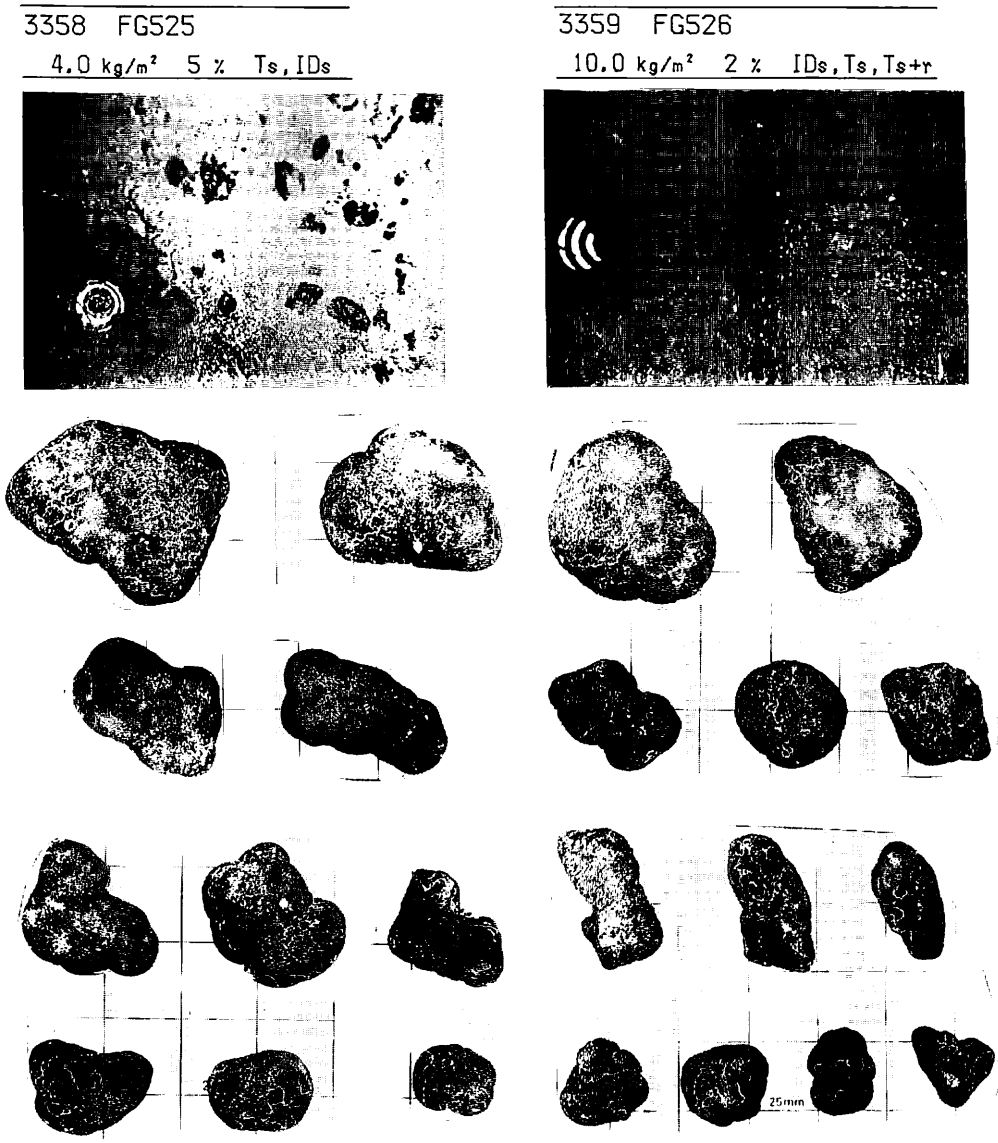

Appendix X-2 (continued)

3360 FG527

4.9 kg/m² 0 % Sr,Dr

3361 FG528

10.5 kg/m² 2 % Sr,Dr

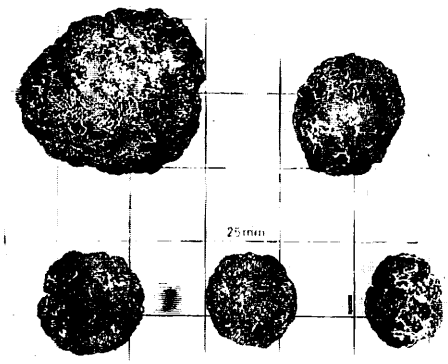

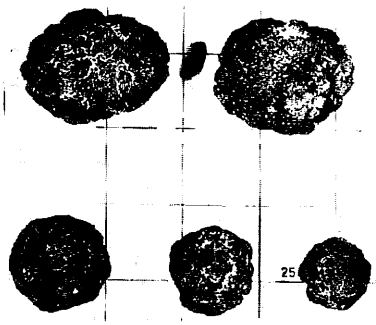

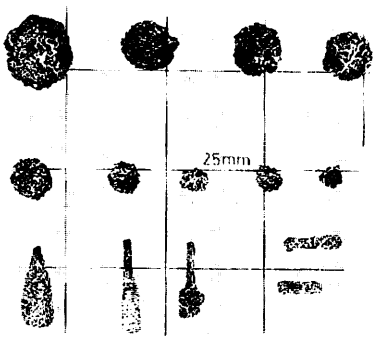

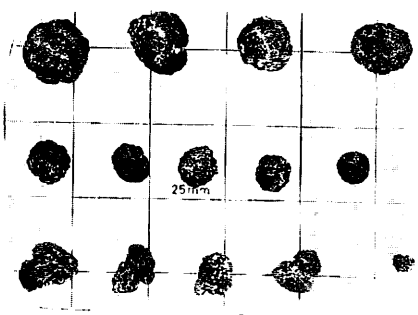

3360 P351

Appendix X-2 (continued)

3362 FG529

10.1 kg/m² 5 % Ssr, SPsr

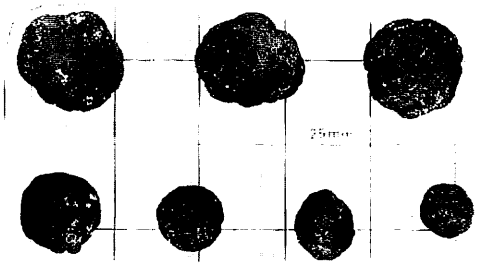

3363 FG530

0.0 kg/m² – –

3364 FG531

11.6 kg/m² 2 % ISs

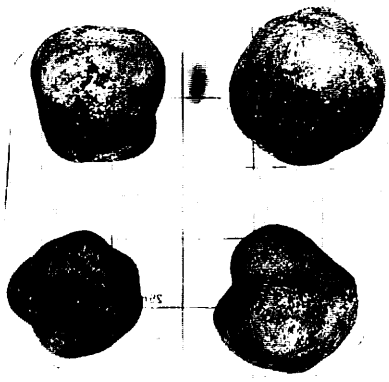

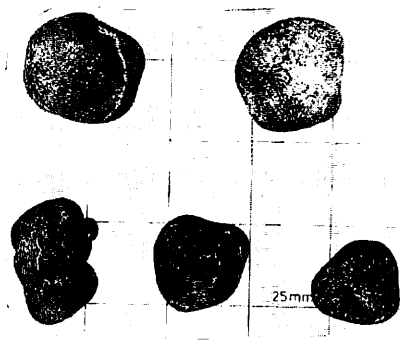

Appendix X-2 (continued)

3365 FG532

10.8 kg/m² 5 % IDs, Ts, IDPs

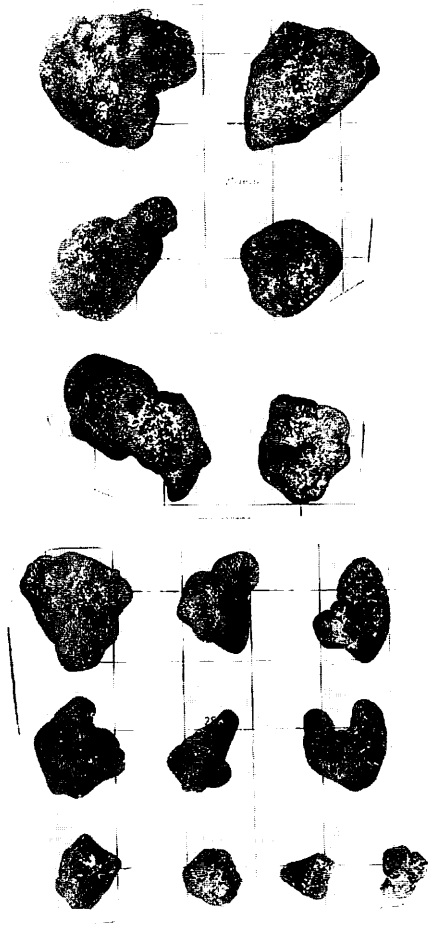

3366 B81

10.1 kg/m² 7 % SPs, Ss

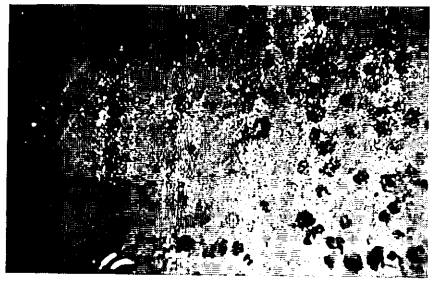

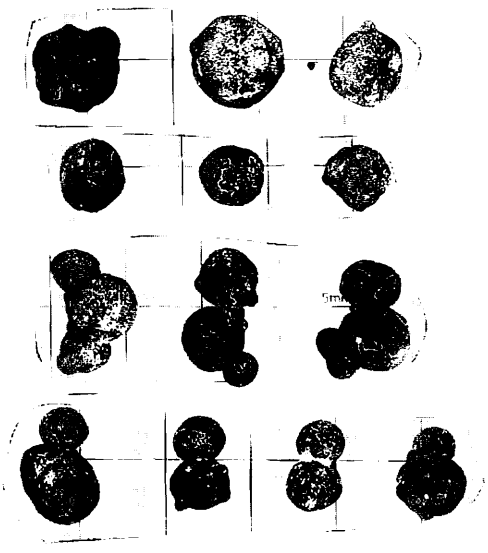

Appendix X-2 (continued)

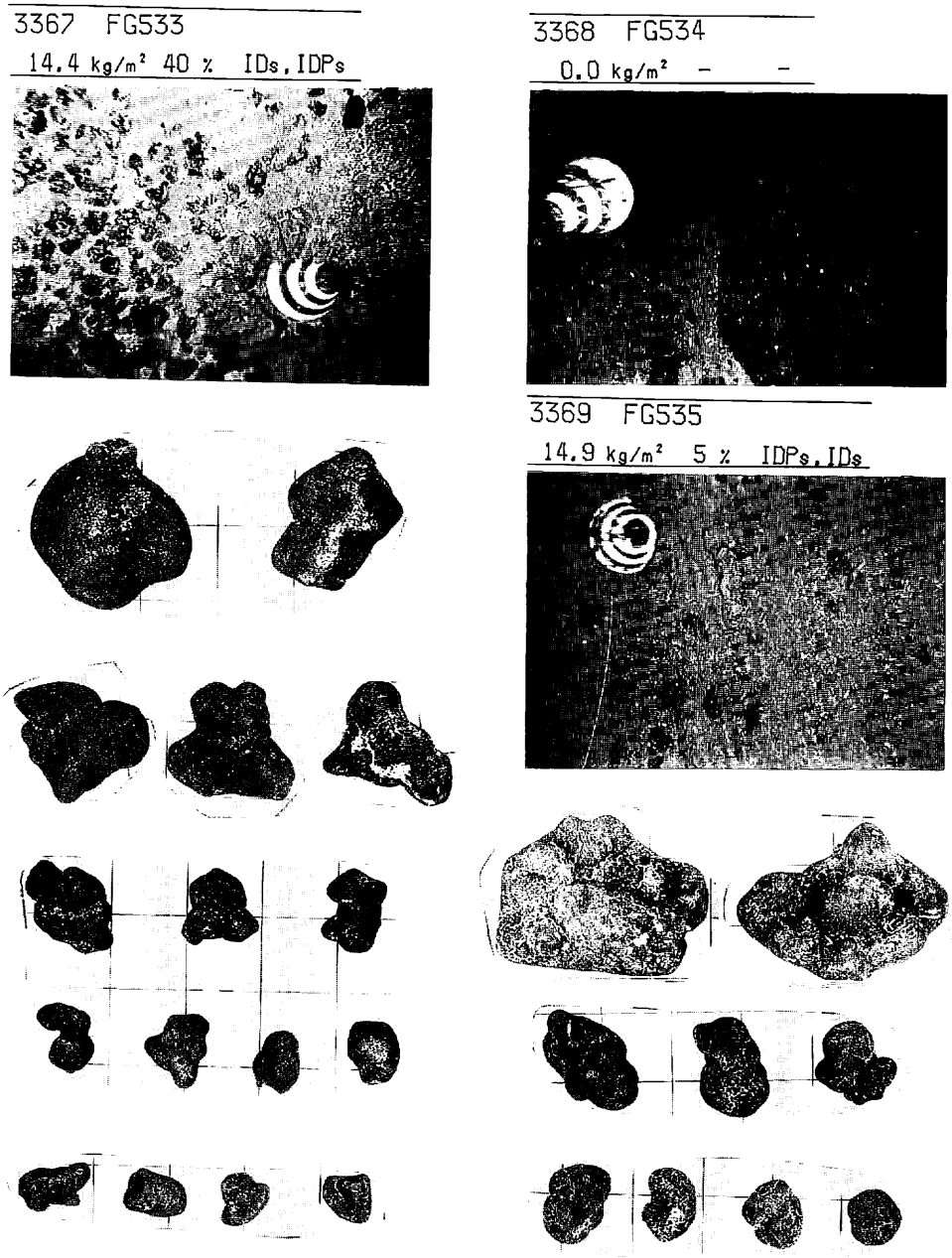

Appendix X-2 (continued)

3370 FG536

0.0 kg/m² 0 % –

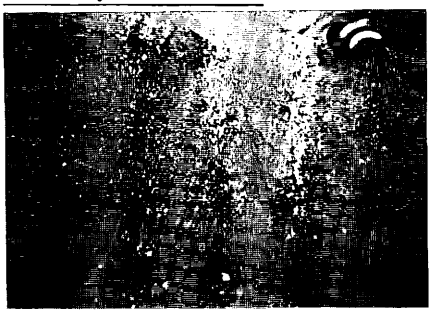

3373 FG539

10.5 kg/m² 5 % IDs, IDPs

3371 FG537

0.0 kg/m² 0 % –

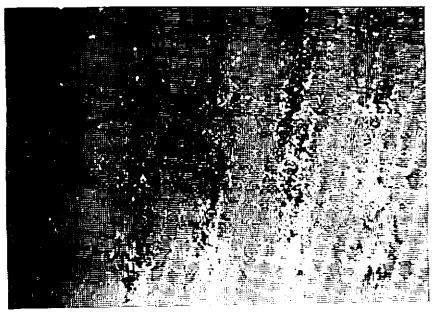

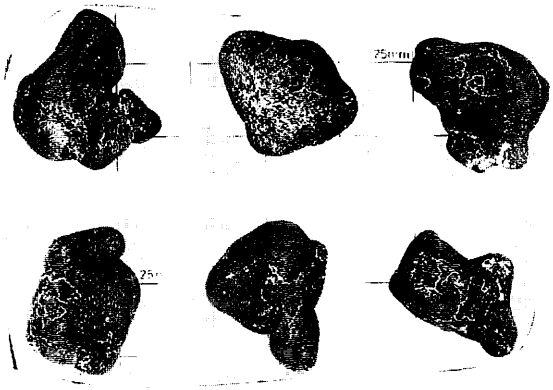

3372 FG538

0.0 kg/m² 0 % –

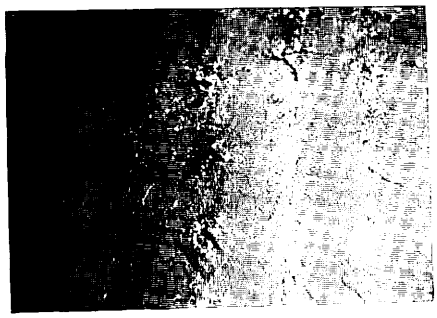

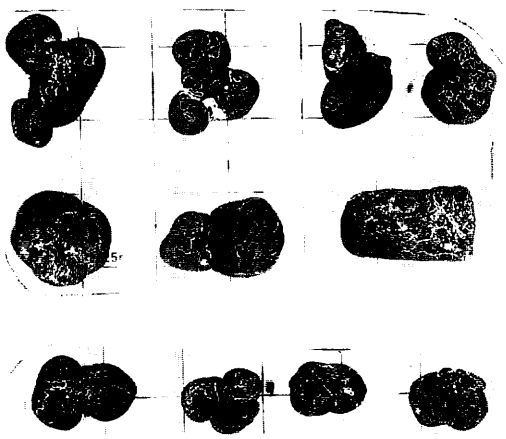

3372 P352

– – –

Appendix X-2 (continued)

3374 FG540

6.5 kg/m² 8 % IDs, IDPs

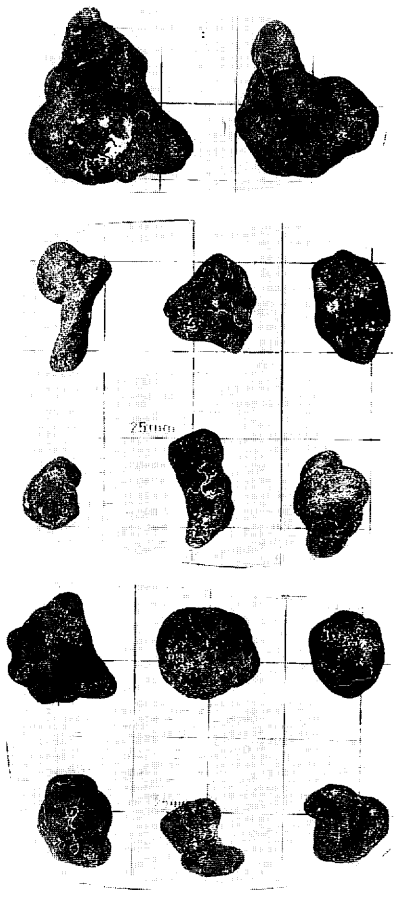

3375 FG541

23.1 kg/m² 10 % ISs, IDs

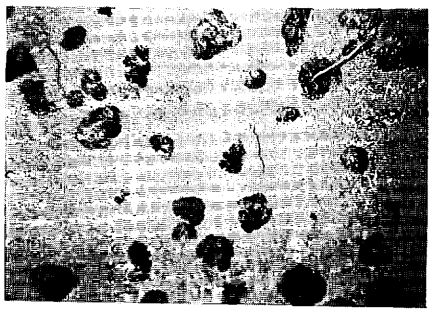

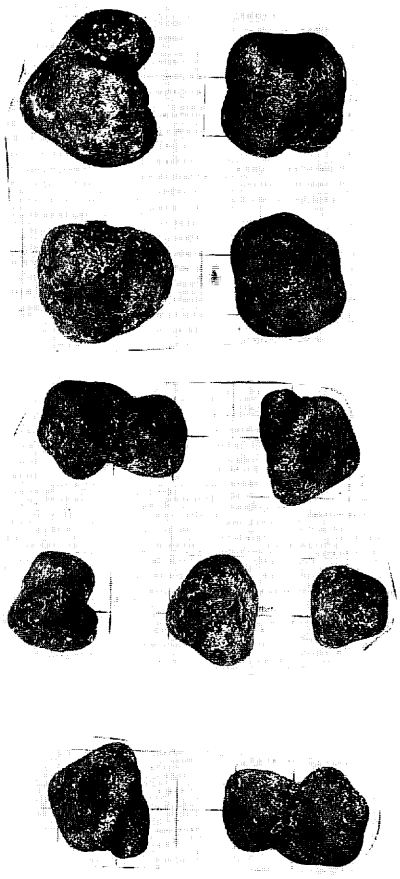

Appendix X-2 (continued)

3376 FG542

18.3 kg/m² 5 % IDs, ISs, IDPs

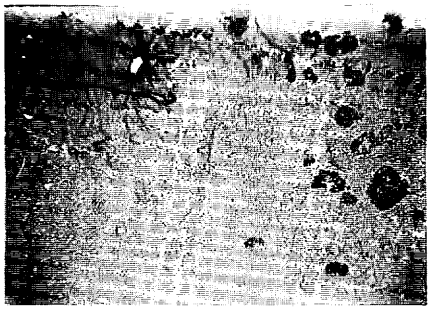

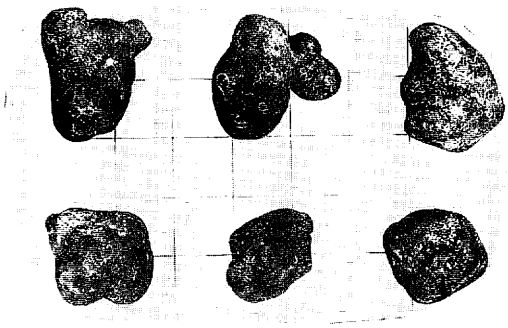

3377 FG543

2.3 kg/m² 0 % Is·r, Fs·r

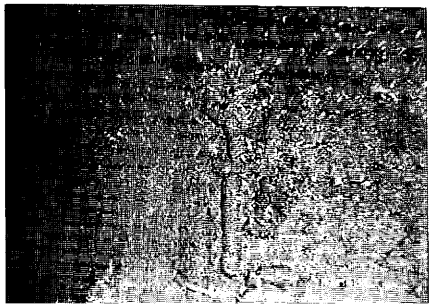

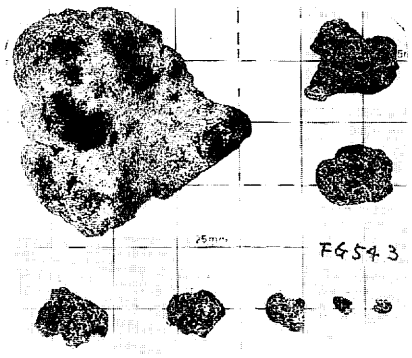

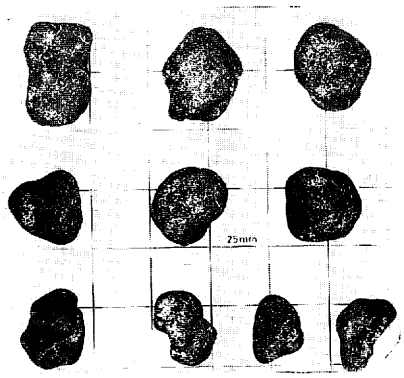

3378 B82

6.3 kg/m² 1 % Ss·r, SPs·r, Ds·r

Appendix X-2 (continued)

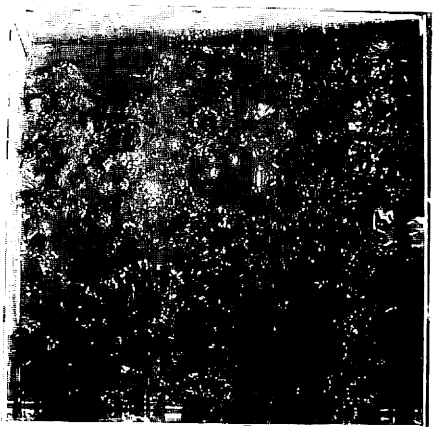

box core surface

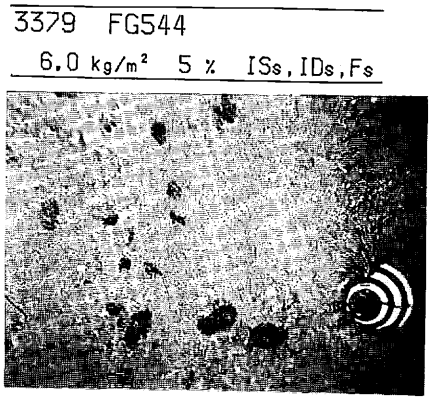

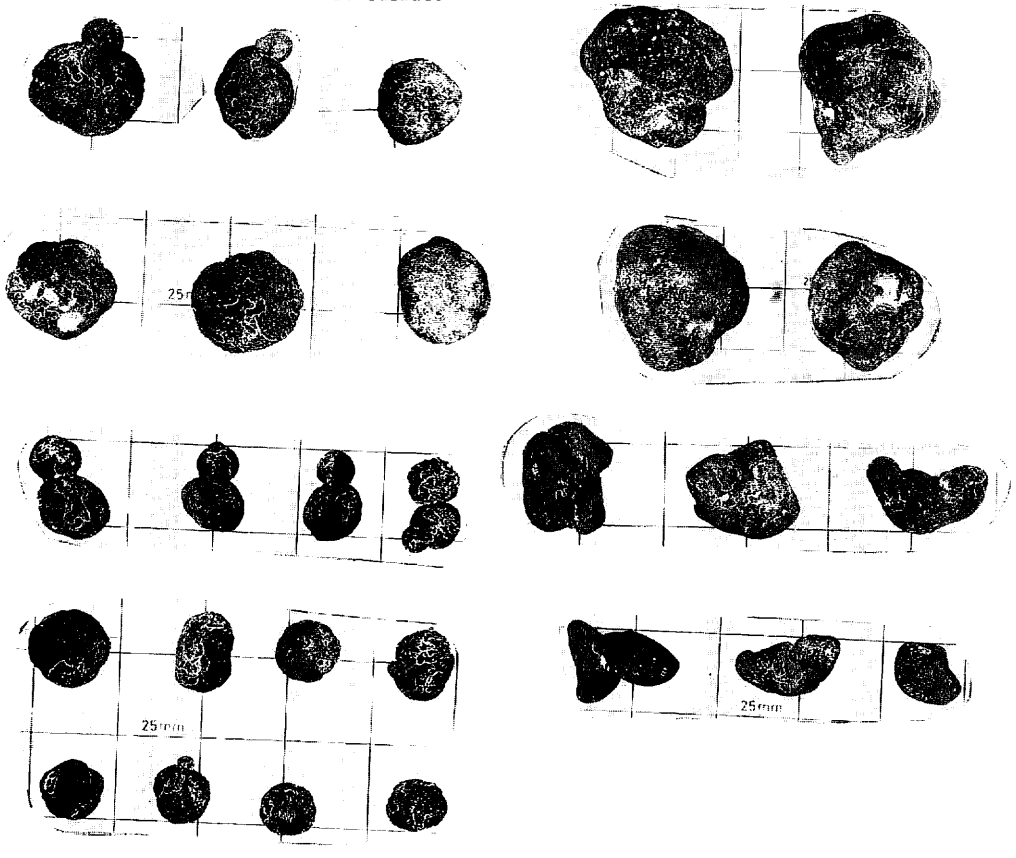

Appendix X-2 (continued)

3380 FG545

0.1 kg/m² 0 % Sr

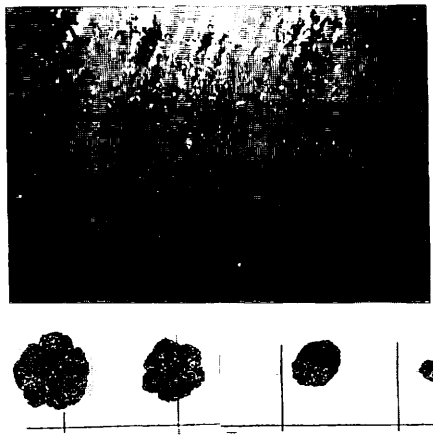

3381 FG546

1.9 kg/m² 2 % IDs, Fs

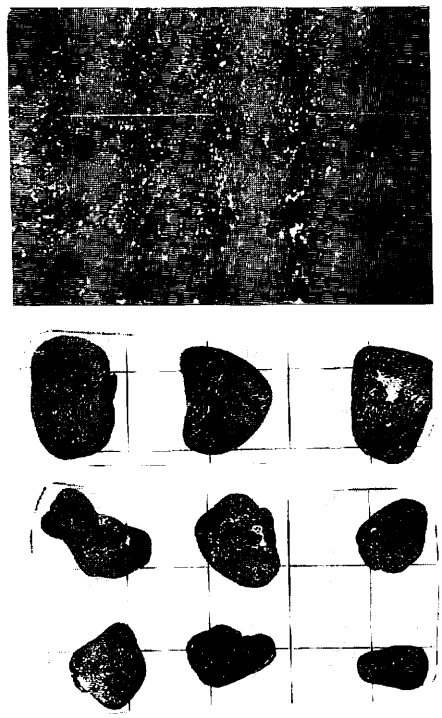

3382 FG547

0.0 kg/m² – –

3383 FG548

13.2 kg/m² 5 % SPs, ISPs

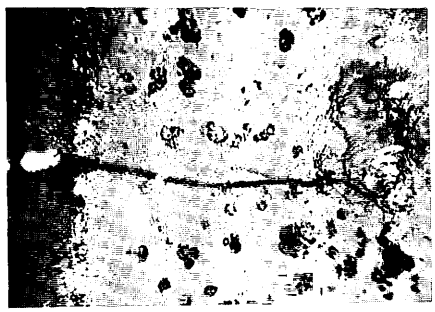

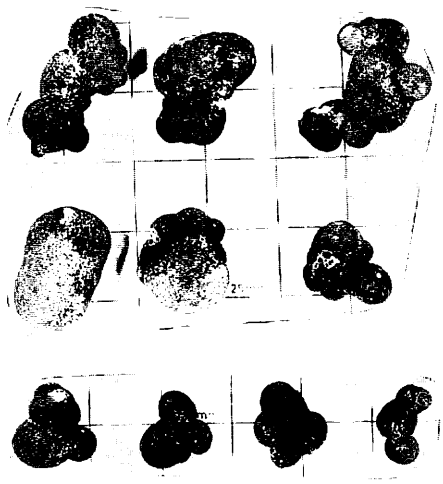

Appendix X-2 (continued)

3383 P353

\- - IDs, IDPs, ISPs

3384 FG549

13.8 kg/m² 2 % IDPs, ISPs, IDs

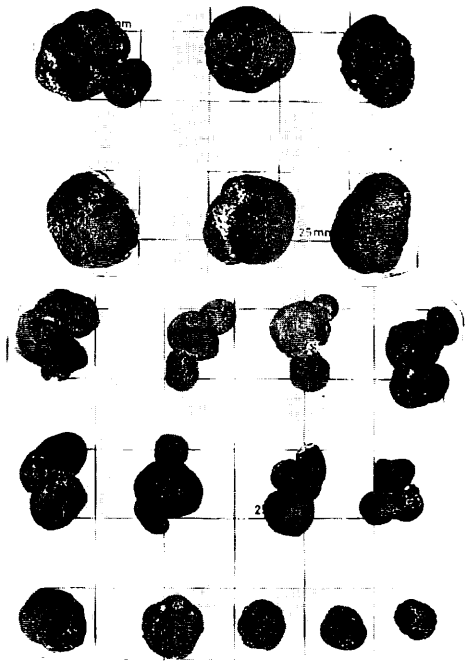

3385 FG550

0.0 kg/m² 0 % (Is)

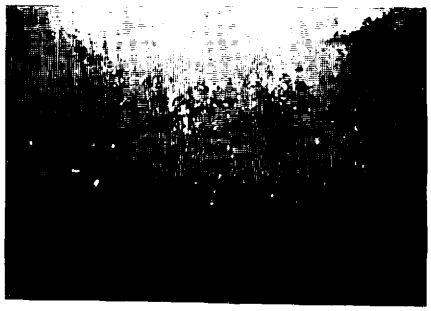

3386 FG551

0.0 kg/m² 0 % Sr

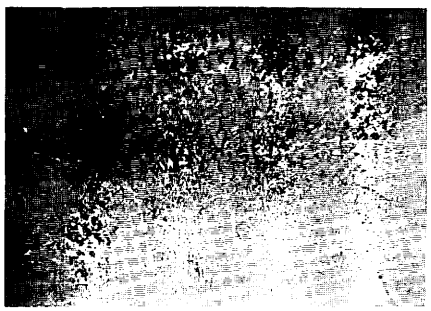

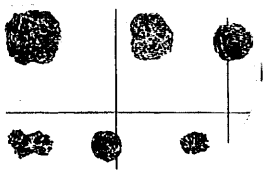

Appendix X-2 (continued)

3387 FG552

1.1 kg/m² 0 % Sr,Dr

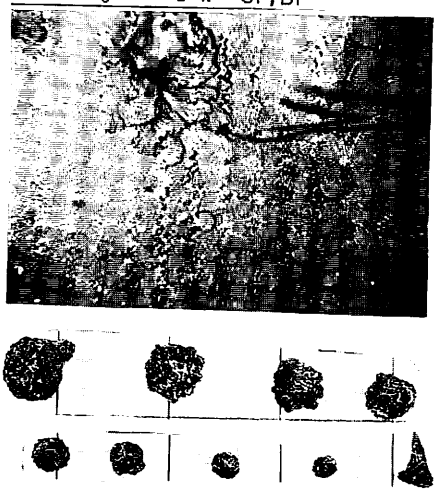

3389 FG553

1.1 kg/m² 4 % (Tr,Vr)

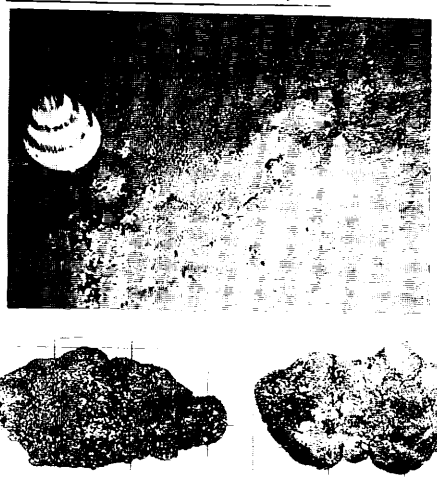

3388 B83

1.0 kg/m² - Sr

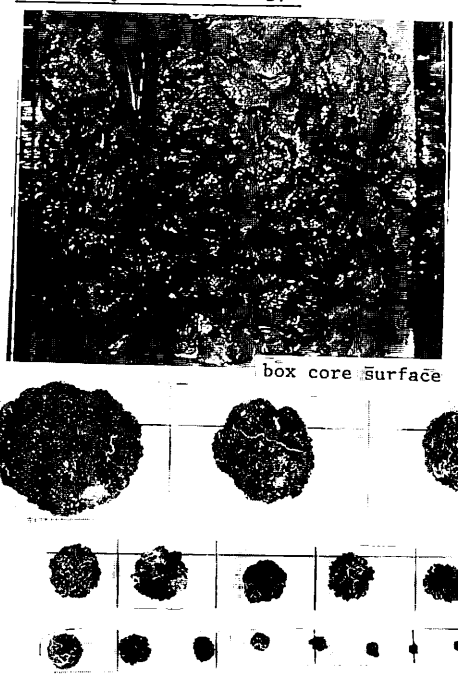

3390 FG554

0.7 kg/m² 0 % Sr

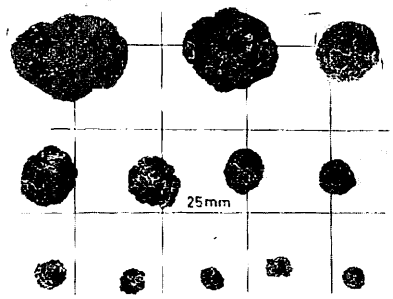

Appendix X-2 (continued)

3391 FG555

0.0 kg/m² 0 % (Vr)

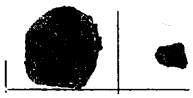

3392 FG556

0.2 kg/m² 0 % Vr, Sr

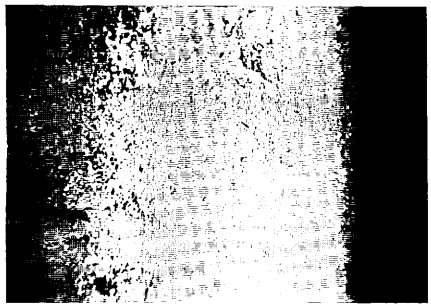

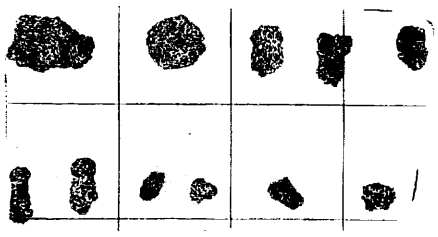

3393 FG557

0.1 kg/m² 0 % Sr, Vr, Fr

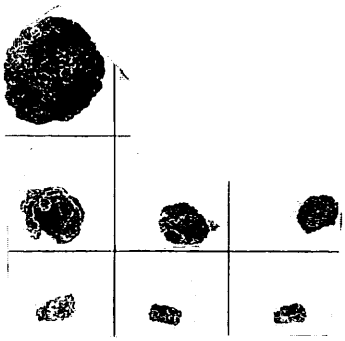

3394 P354

– – –

3395 FG558

0.0 kg/m² 0 % –

Appendix X-2 (continued)

3396 FG559

0.0 kg/m² 0 % –

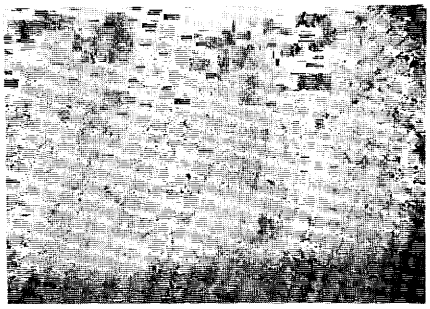

3398 FG561

5.6 kg/m² 20 % ISs, IDs, Fs

3397 FG560

0.3 kg/m² 0 % Fsr, Sr

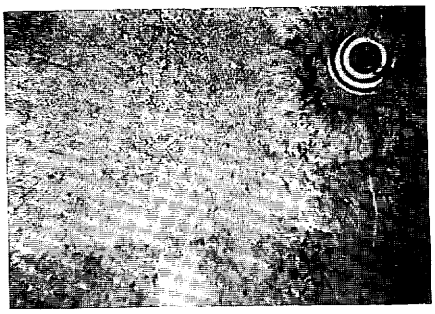

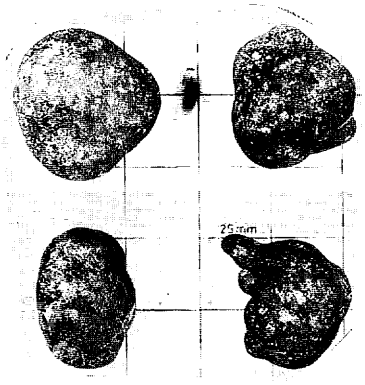

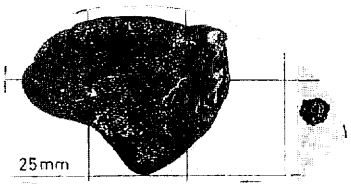

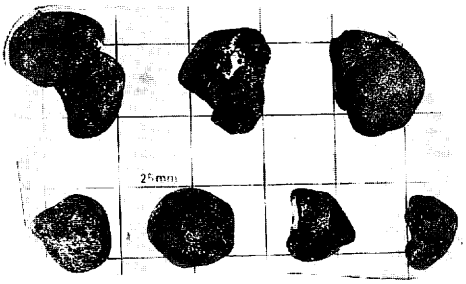

Appendix X-2 (continued)

3399 B84

11.8 kg/m² 10 % IDPs, IDs

box core surface

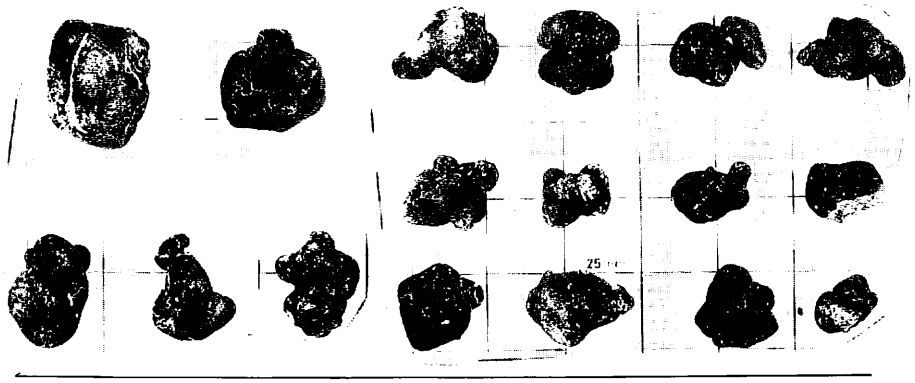

3399 B84X

3.8 kg/m² - IDPs, IDs

buried at 16 cm depth

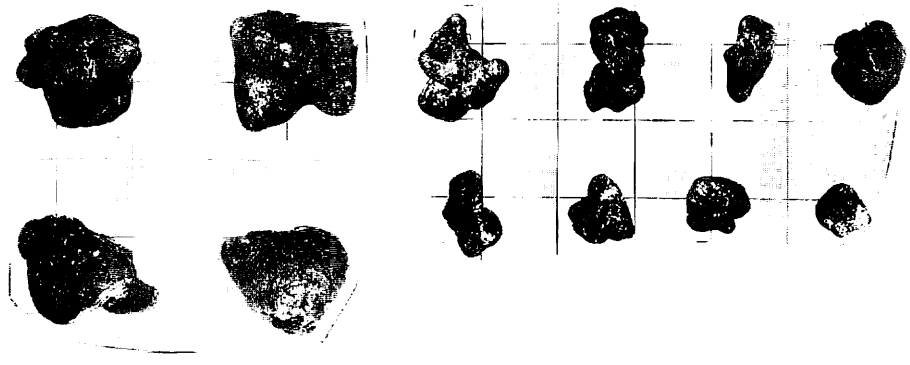

Appendix X-2 (continued)

3400 P355

– – IDs

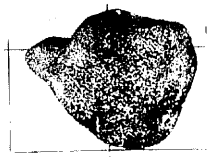

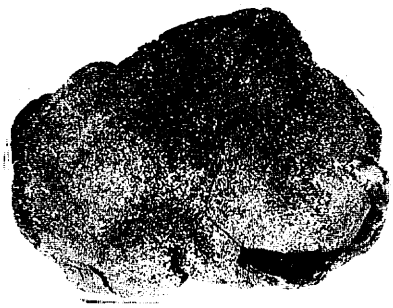

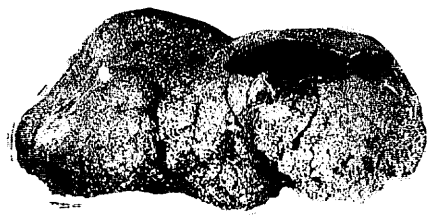

3402 FG562

1.2 kg/m² 2 % ISs, IDs

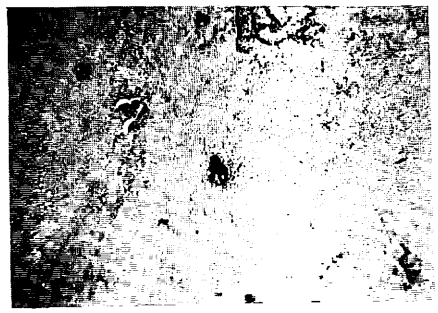

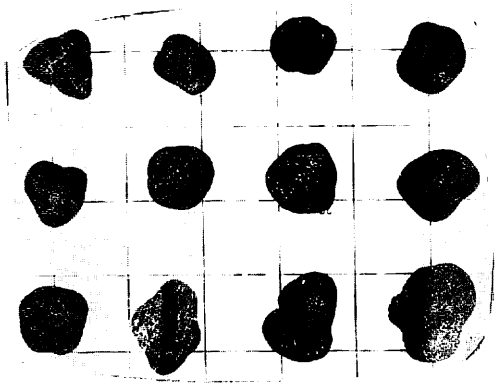

3403 D514

– – SPs·r, Ss·r

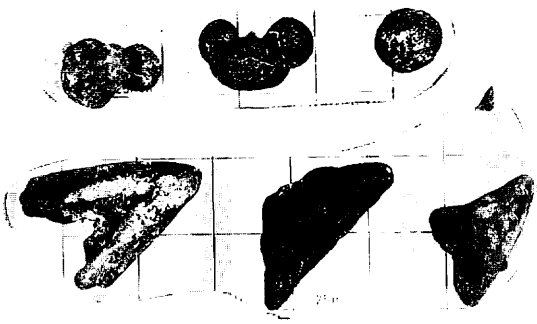

Appendix X-2 (continued)

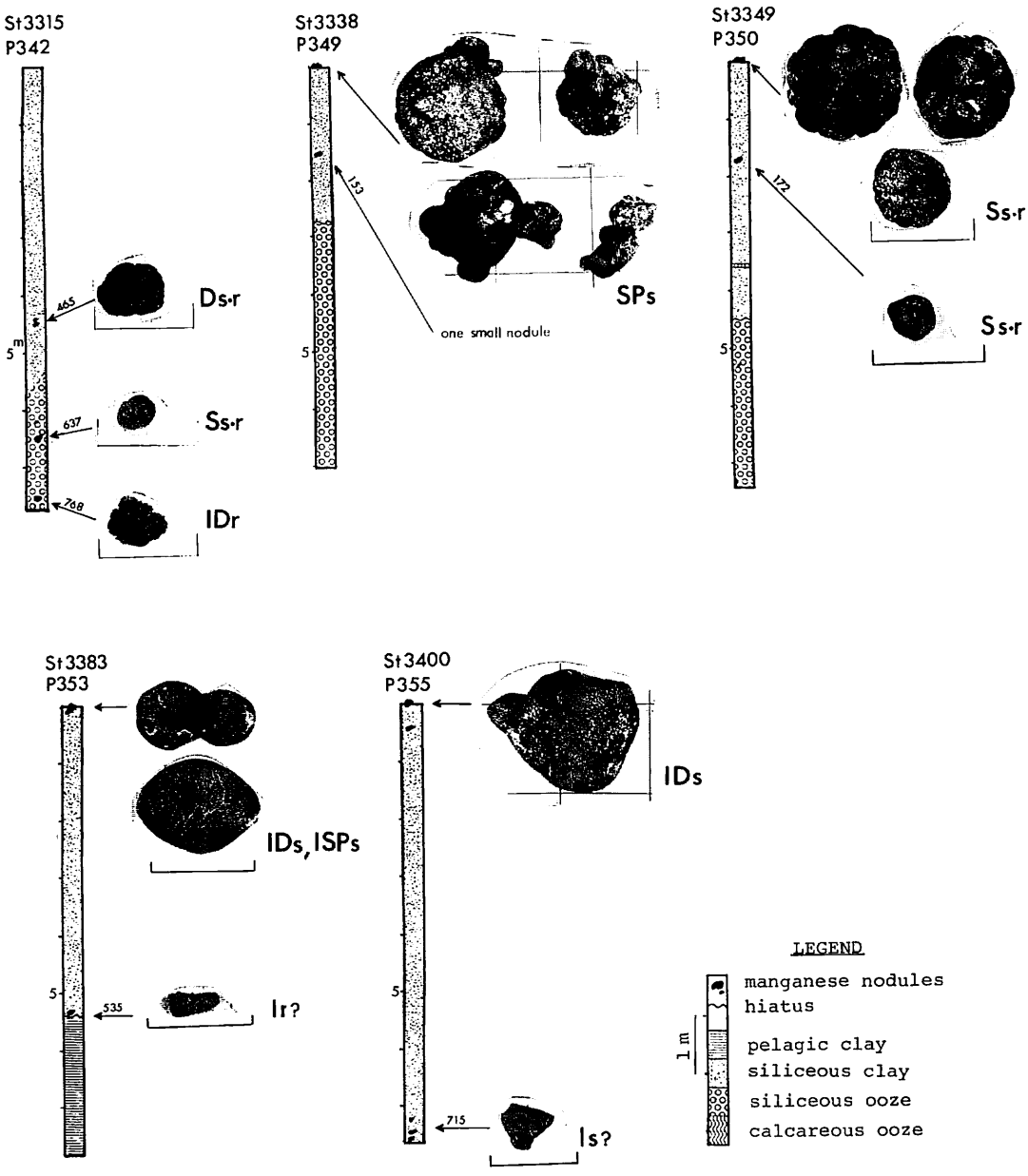

Appendix X-3 Manganese nodules buried deep within piston cores and box cores. Lithological description by Nishimura and Ikehara (chapter VI of this volume). Scale bar with nodules: 25 mm. Depth of buried nodules shown with arrows in cm.